

Western  Graduate&PostdoctoralStudies

Western University
Scholarship@Western

Electronic Thesis and Dissertation Repository

12-18-2013 12:00 AM

Performance assessment of wireless Two Way Relay Channel systems

Siramack Ghadimi
The University of Western Ontario

Graduate Program in Electrical and Computer Engineering
A thesis submitted in partial fulfillment of the requirements for the degree in Doctor of Philosophy
© Siramack Ghadimi 2013

Follow this and additional works at: <https://ir.lib.uwo.ca/etd>



Part of the [Other Electrical and Computer Engineering Commons](#)

Recommended Citation

Ghadimi, Siramack, "Performance assessment of wireless Two Way Relay Channel systems" (2013).
Electronic Thesis and Dissertation Repository. 1845.
<https://ir.lib.uwo.ca/etd/1845>

This Dissertation/Thesis is brought to you for free and open access by Scholarship@Western. It has been accepted for inclusion in Electronic Thesis and Dissertation Repository by an authorized administrator of Scholarship@Western. For more information, please contact wlsadmin@uwo.ca.

Performance assessment of wireless Two Way Relay Channel systems

(Thesis format: Monograph)

by

Siamack Ghadimi

Graduate Program
in
Engineering Science
Electrical and Computer Engineering

A thesis submitted in partial fulfillment
of the requirements for the degree of
Doctor of Philosophy

School of Graduate and Postdoctoral Studies
Western University
London, Ontario, Canada

© Siamack Ghadimi December 2013

Abstract

The objective of this thesis is theoretical investigations and numerical simulations of Two Way Relay Channel (TWRC) systems, particularly in an impulsive noise environment. Special attention is given to investigation of a TWRC system based on polarized antennas.

The first part of the thesis focuses on modeling of impulsive noise and the effect of impulsive noise on TWRC systems. The study was conducted by simulating the wireless TWRC models in the presence of impulsive noise. The bit error probability performance of the channel data was compared and at last their results are shown by graphs.

The study has been further extended to multi antenna TWRC systems. Simulation analysis of multi antenna TWRC systems in an impulsive noise environment was conducted by using a MISO Alamouti scheme and a MIMO system.

The second part of the thesis dedicated to investigation of TWRC polarization systems. A new TWRC scheme based on polarized antennas has been proposed and simulated. By polarization we are able to achieve higher spectral efficiency through the use of spatial multiplexing, and improve the reliability by spatial diversity.

A new network topology based on TWRC polarization systems proposed. It is well suited to mitigate effect of delay in a communication system, particularly for high priority data transmission, or increase reliability of a communication system by redundant transmission.

Acknowledgements

I would like to thank the department of Electrical and Computer Engineering at Western University. I am grateful to Doug Campbell for his thoughtful editing of my thesis.

Contents

| | |
|--|------------|
| Abstract | ii |
| Acknowledgements | iii |
| Table of Contents | iv |
| List of Tables | vi |
| List of Figures | vii |
| Acronyms | ix |
| 1 Introduction | 1 |
| | |
| I Impulsive noise and wireless Two Way Relay Channel system | 6 |
| | |
| 2 Impulsive noise | 7 |
| 2.1 Introduction | 7 |
| 2.1.1 Literature review | 7 |
| 2.2 Characteristic of Impulsive noise | 10 |
| 2.2.1 Impulsive noise channel models for wireless system | 11 |
| 2.3 Conclusions | 14 |
| | |
| 3 Wireless Two Way Relay Channel system | 15 |
| 3.1 Introduction | 15 |
| 3.2 Network coding | 15 |
| 3.3 System model | 17 |
| 3.3.1 Error probability analysis | 19 |
| 3.4 Simulations and results | 23 |
| 3.4.1 TWRC vs. AF: | 23 |
| 3.4.2 BEP as function of SNR | 25 |
| 3.4.3 BEP as function of SIR | 27 |
| 3.4.4 BEP as function of SNR and SIR | 29 |
| 3.4.5 Viterbi decoding algorithm | 30 |

| | | |
|-----------|--|-----------|
| 3.4.6 | Adaptive Coding and Modulation | 31 |
| 3.5 | Conclusions | 37 |
| 4 | Multi antennas in a wireless TWRC system | 39 |
| 4.1 | Introduction | 39 |
| 4.2 | System model of Multiple-Input and Single-Output TWRC | 39 |
| 4.2.1 | Error probability analysis | 43 |
| 4.2.2 | Simulations and results | 50 |
| 4.3 | System model of Multiple-Input and Multiple-Output TWRC | 53 |
| 4.3.1 | Simulations and results | 54 |
| 4.4 | Conclusions | 55 |
| | | |
| II | Polarization | 56 |
| | | |
| 5 | Polarized antennas in a wireless TWRC system | 57 |
| 5.1 | Introduction | 57 |
| 5.2 | Polarized Antenna Network Coding (PANC) and full duplex PANC | 57 |
| 5.3 | System model | 60 |
| 5.3.1 | Full duplex PANC error probability analysis | 67 |
| 5.3.2 | Simulations and results | 74 |
| 5.4 | TWRC polarization diversity | 80 |
| 5.5 | Polarized Multicast Two Way Relay Channel (PM-TWRC) | 84 |
| 5.5.1 | Polarized Multi Path TWRC (PMP-TWRC) | 85 |
| 5.6 | Conclusions | 86 |
| | | |
| 6 | Conclusions and future work | 87 |
| | | |
| | Curriculum Vitae | 99 |

List of Tables

| | | |
|-----|--|----|
| 3.1 | Case study of constellations types | 37 |
| 4.1 | Values of $\bar{\alpha}_{m,n}$ | 48 |

List of Figures

| | | |
|------|--|----|
| 1.1 | Noise and interference in a wireless TWRC system | 3 |
| 1.2 | Jamming in a wireless TWRC system | 4 |
| 2.1 | Character of Impulsive noise | 10 |
| 2.2 | Gaussian and impulsive noise channel | 12 |
| 3.1 | Network coding | 16 |
| 3.2 | System Model for a Two Way Relay Channel | 17 |
| 3.3 | Constellation of received signal at the relay node | 20 |
| 3.4 | TWRC vs. AF relay system | 24 |
| 3.5 | TWRC system while SIR=5 dB | 26 |
| 3.6 | TWRC system while SIR=10 dB | 26 |
| 3.7 | TWRC system while SIR=15 dB | 26 |
| 3.8 | TWRC system varying SIR while SNR = 15 dB | 27 |
| 3.9 | TWRC system while SNR=5 dB | 28 |
| 3.10 | TWRC system while SNR=10 dB | 28 |
| 3.11 | TWRC system while SNR=15 dB | 28 |
| 3.12 | TWRC system varying SIR and SNR while $p= 0.5$ | 29 |
| 3.13 | TWRC system with the Viterbi decoding | 30 |
| 3.14 | An asymmetric TWRC system | 31 |
| 3.15 | Constatation at relay for asymmetric TWRC BPSK and QPSK modulation | 32 |
| 3.16 | Asymmetric modulation of TWRC | 33 |
| 3.17 | Asymmetric modulation of TWRC when $ h_1 = h_2 $ | 34 |
| 3.18 | Optimal decision decoding algorithm (ODDA) for an asymmetric TWRC | 36 |
| 3.19 | Case study of constellation types for an asymmetric TWRC | 37 |
| 4.1 | A MISO TWRC system | 40 |
| 4.2 | Upper and lower bounds when $p = 0$ and SIR = 10 dB | 50 |
| 4.3 | Upper and lower bounds when $p = 1$ and SIR = 10 dB | 50 |
| 4.4 | Upper and lower bounds when $p = 0$ and SNR = 5 dB | 51 |
| 4.5 | Upper and lower bounds when $p = 1$ and SNR = 5 dB | 51 |
| 4.6 | Performance comparison of different systems, SIR = 10 dB | 52 |
| 4.7 | A MIMO TWRC system | 53 |
| 4.8 | MIMO TWRC system vs. MISO TWRC system | 55 |
| 5.1 | Network coding | 58 |

| | | |
|------|--|----|
| 5.2 | Network coding as function of time | 59 |
| 5.3 | Polarized wave and scatter | 61 |
| 5.4 | Geometry for the two-ray propagation model | 64 |
| 5.5 | A cross-polarized channel | 66 |
| 5.6 | System model for a wireless TWRC full duplex PANC | 67 |
| 5.7 | Cross-polarized system vs. full duplex system | 75 |
| 5.8 | Bit error probability as a function of SNR for different K-factor for SNR = 10 dB | 77 |
| 5.9 | Bit error probability as a function of K-factor | 78 |
| 5.10 | Polarization rotation angle | 79 |
| 5.11 | CDF function of XPD | 80 |
| 5.12 | XPD function of antenna rotation angle | 80 |
| 5.13 | Comparison of MIMO cross-polarized antenna TWRC with MIMO TWRC scenarios, k=0 | 82 |
| 5.14 | Comparison of cross-polarized TWRC with MIMO 2X2 TWRC, k=0 | 83 |
| 5.15 | Unicast system vs. multicast system | 85 |

Acronyms

| | |
|-------------|--|
| ACM | <i>Adaptive Coding and Modulation</i> |
| AF | <i>Amplify and Forward</i> |
| AM | <i>Asymmetric Modulation</i> |
| ANC | <i>Analogue Network Coding</i> |
| AWGN | <i>Additive White Gaussian Noise</i> |
| BC | <i>Broadcast Channel</i> |
| BEP | <i>Bit Error Probability</i> |
| CF | <i>Characteristic Function</i> |
| CSI | <i>Channel State Information</i> |
| DNC | <i>Digital Network Coding</i> |
| LOS | <i>Line Of Sight</i> |
| MAC | <i>Multiple Access Channel</i> |
| MIMO | <i>Multiple-Input and Multiple-Output</i> |
| MISO | <i>Multiple-Input and Single-Output</i> |
| ML | <i>Maximum Likelihood</i> |
| NC | <i>Network Coding</i> |
| NLOS | <i>Non Line Of Sight</i> |
| PANC | <i>Polarized Antenna Network Coding</i> |
| PDF | <i>Probability Density Function</i> |
| PLC | <i>Power Line Communication</i> |
| SEP | <i>Symbol Error Probability</i> |
| SIMO | <i>Single-Input and Multiple-Output</i> |
| SIR | <i>Signal-to-Impulsive-noise Ratio</i> |
| SNR | <i>Signal-to-Noise Ratio</i> |
| TWRC | <i>Two Way Relay Channel</i> |
| XPD | <i>Channel cross-Polarization Discrimination</i> |

Chapter 1

Introduction

The future demands calling for more robust and reliable communication systems, and demanding higher spectral efficiency, network bandwidth and capacity, lower energy consumption, and higher mobility.

To achieve these requirements, we need to have a robust wireless communication systems which should work in a dense Electro Magnetic (EM) environment. Two way communication systems appear a logical choice to satisfy these demands.

Generally, the two most fundamental requirements that need to be considered for a two way communication system are the throughput of the channel, often called the speed or bandwidth, and the latency of the channel, or delay. Secondary, but important, considerations are reliability and security.

The fundamental goals of the two way communication system for the future demands according to the following principles can be defined as:

1. Have a full two-way real-time digital communication with high throughput or capacity for all kinds of information between all participants in the smart cities.
2. Have low delay.
3. Be able to adapt to any kind of architecture and cover the entire length and breadth of all types of communication scenarios.
4. Have a distributed architecture.

5. Be stable and reliable against failures, noise, interference, and perform continuous self-assessments to detect and analyze matters.
6. Be robust, self-configuring, self-healing, self-upgrading and support future technology. Hence have capability to adapt to any changes in future topology without requiring termination of data transmission.
7. Be secure.
8. Be easy to install (plug-and-play) and cost effective to maintain.

Studies have shown there exist different ways of propagating and transmitting man-made noise¹ through wireless communication systems. One of the most common ways is Electro Magnetic Interference (EMI) generated by an antenna.

The wireless systems are subjected to interference from any electromagnetic sources, and the signal strength is greatly reduced by many materials. The presence of items such as microwave ovens, DECT phones, electrical doors, elevators, remote-control toys, machinery, electrical terrain, and many other things in the local environment will dramatically reduce the throughput and reliability of the system, see Figure 1.1. In a Two Way Relay Channel (TWRC) system [5], network coding can improve the system throughput by %100 [6].

The outage of the communication system for example jamming², failure, natural catastrophes, attacks, etc. will directly impact the application utilizing the communication system.

1. Man-made noise means noise generated by electrical equipment, [1], [2], [3] and [4].

2. Jamming means when somebody purposely sends signals with the same frequency as the desired signal to a network to interfere with and disrupt the operation of the network.

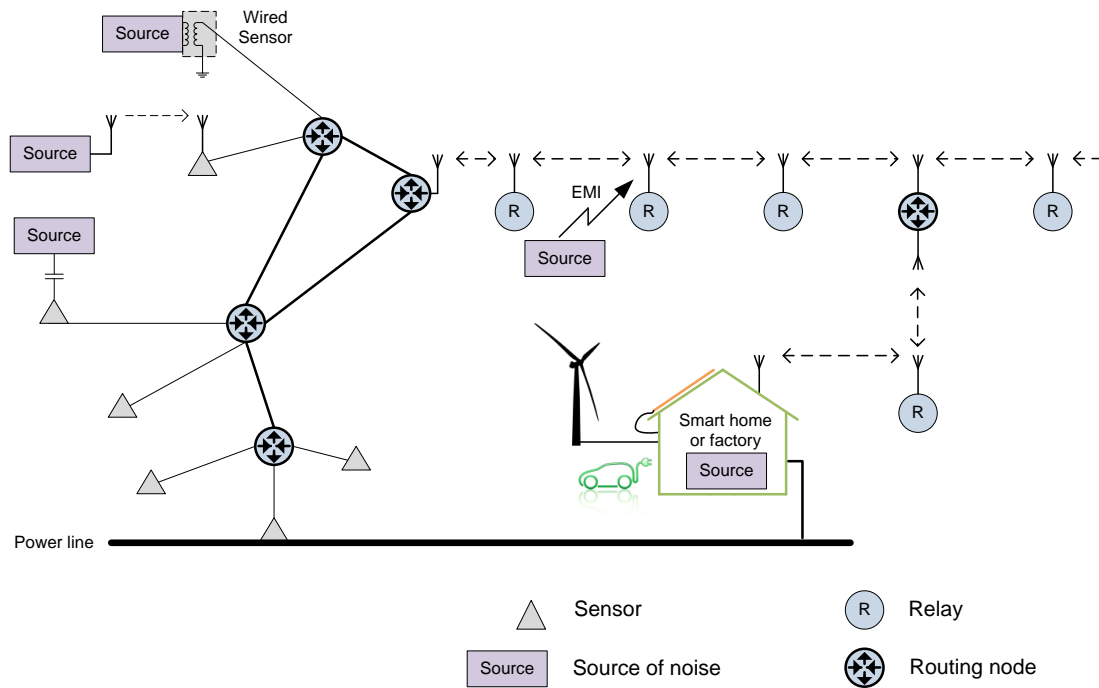


Figure 1.1: Noise and interference in a wireless TWRC system

The TWRC system however, will be able to continue functioning if some node(s) or some communication channel(s) fail(s), because a relay algorithm will detect, raise an alarm and choose to send signals through other available path(s), known as ‘surviving path(s)’ or ‘node(s)’, Figure 1.2.

In the case of jamming, there are other ways to prevent jamming in the wireless system such as Spread-Spectrum methods³ i.e. Direct Sequence Spread Spectrum

3. Spread-spectrum techniques are methods by which a signal generated with a particular bandwidth is deliberately spread in the frequency domain, resulting in a signal with a wider bandwidth.

(DSSS)⁴ technique [7], Frequency Hopping (FH)⁵ technique, and Code Division Multiple Access (CDMA)⁶ technique, [8], [9], [10].

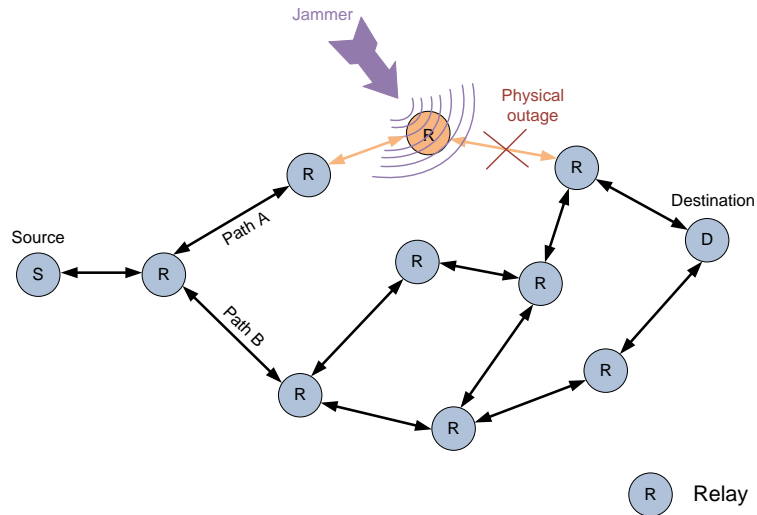


Figure 1.2: Jamming in a wireless TWRC system

The wireless system discussed until now leads to an analysis of the gaps in research related to TWRC system in the following Chapters.

The major contributions from this thesis are:

Theoretical and performance analysis of a single antenna and multiple antennas TWRC system in an impulsive noise environment.

4. In DSSS, the data is multiplied with a pseudo-noise (PN) sequence to create a longer sequence. Since the PN sequence is like noise, it is inherently wideband and, as a result, it spreads the spectrum of the data sequence too, to create a noise like sequence. Because the sequence is spread over a large band, it is less prone to interference, while it has noise-like character, which makes it difficult to detect.

5. In FH, when a node detects attacks on the current frequency, it will jump to the next available frequency. Or hop over multiple frequencies together regardless of the presence of attackers.

6. CDMA is a channel access method used by various radio communication technologies. CDMA is a property of direct-sequence spread spectrum (DSSS), which allows multiple transmitters to share the same channel within the limits of the cross-correlation properties of their pseudonoise (PN) sequences.

A new algorithm called Optimal Decision Decoding Algorithm (ODDA) for an asymmetric TWRC system.

A new TWRC scheme based on polarized antennas.

Diversity polarization for a polarized antennas TWRC system.

A new network topology based on the polarized antennas TWRC system.

Part I

Impulsive noise and wireless Two Way Relay Channel system

Chapter 2

Impulsive noise

2.1 Introduction

Implementation of wireless TWRC system depends on the efficiency and reliability of channel capabilities. The measurements [11] have shown that in the real world background noise e.g. impulsive noise, has a direct impact on channel quality and capacity.

Most wireless communication systems are designed for voice, video, and internet data transmission and they are tolerant to errors caused by impulsive noise. This kind of error is not tolerable for sensitive data communication such as industrial control data. Thus impulsive noise channel models for wireless systems are important in determining the error rate for the design of a robust system.

2.1.1 Literature review

Edward N. Skomal [12], has carefully studied natural and man-made radio noise. According to him, man-made radio interference is a serious problem, which has an impact on everything from air travel and ship navigation to heart pacemakers and car radios. It is a part of our environment and it increases as our society becomes more computer/electrical equipment oriented.

J. D. Parsons [13], explains that impulsive noise is more important to the degradation of a signal than Gaussian noise in high frequencies.

Andrew B. Bodonyi [14] has studied and presents a review of several reference papers, which show measurements of impulsive noise for frequencies from 3 kHz up to 4 GHz, he says:

Considerable work has been done in analyzing the performance of digital data communications channels, under the influence of Gaussian noise. This is not too difficult, since the theoretical tools as well as the experimental ones are well known and easy to handle. Unfortunately the results are, in many cases, not in close agreement with the error rates of practical communication channels. A closer investigation reveals that over the majority of long haul communication circuits the major source of additive disturbance is essentially non-Gaussian, that is, its probability cannot be closely approximated by the Gaussian distribution. Due to the relatively frequent occurrence of high amplitude, short duration noise peaks, this type of noise was characterized as impulsive noise. Such impulsive noise is experienced in a wide range of communications media.

Kenneth L. Blackard [15], has investigated characteristics, sources and the average of impulsive noise measurements inside several office buildings and retail stores. The receiver for measurements operated at 918 MHz, 2.44 GHz, and 4.0 GHz with a nominal 40 MHz, 3 dB RF bandwidth. Statistical analysis of the measurements are presented in the form of noise level distributions, amplitude probability distributions, pulse duration distributions, and inter-arrival time distributions. The results display devices with electromechanical switches, such as electric motors in elevators, copy machines, printers, etc and microwave ovens, which are principal

sources of impulsive noise in indoor channels.

Also, examples of impulsive noise sources have been investigated including automobile ignitions [13], [16] microwave ovens [17], [18], photocopier machines [18], fluorescent lights [12] and power lines [12].

Okan Z. Batur [19], Anil Shukla [20], T. Keith Blankenship [21], J. D. Parsons [22], Gunnar Bedicks [23], Ashok Chandra [24], and A.D. Spaulding [25] have measured and showed the effects of impulsive noise and interference in a wide frequency band between 100 kHz to 3GHz for wireless channels. Measurements show that the impulsive noise has been found at 100 kHz to 3GHz.

Kenneth L. Blackard [18], focused on three frequency bands: 918 MHz, 2.44 GHz, and 4 GHz. The measurements took place within five retail stores and office buildings. The result shows that equipment with electromechanical switches, such as electric motors in elevators, refrigeration units, copy machines, printers, etc. are main sources of impulsive noise in indoor environments in the low microwave regime.

R. E. Owen [26], has studied electrical switches, such as Thyristors and Diode-types. These kind of switching devices generate impulsive noise because of the commutation process required to switch the flow of current from one conducting semiconductor to another. This study shows that impulsive noise of such devices at high frequency 3-300 kHz frequency band, may cause interference to digital communication systems.

Vehbi C. Gungor [11], shows the challenges of the wireless sensor networks in a smart grid and depicts a statistical characterization of the wireless channel in different electric-power-system environments. Their field tests were performed on IEEE 802.15.4 compliant sensor nodes (using CC2420 radio chips) in a 500-kV substation, a main power control room, as well as an underground network transformer vault to measure background noise, channel characteristics, and attenuation in the 2.4-GHz

frequency band. Various communication links, including both Line Of Sight (LOS) and Non Line Of Sight (NLOS) scenarios, are also considered. They found the average noise level is around -90 dBm, which is significantly higher than that of outdoor environments, i.e., -105 dBm background noise is found in outdoor environments. They also observed that background noise continuously changes over time, which they assumed can be caused by temperature changes and interference levels. Other good sources that generally describe radio frequency impulsive noise and its effects upon radio receivers can be found in [11], [17], [27–34]

2.2 Characteristic of Impulsive noise

Impulsive noise is graded as manmade noise. The impulsive noise is non-contiguous, consisting of irregular pulses or noise spikes of short duration and of relatively high amplitude as high as several hundred microvolts. Each spike has a broad spectral content, Figure 2.1.

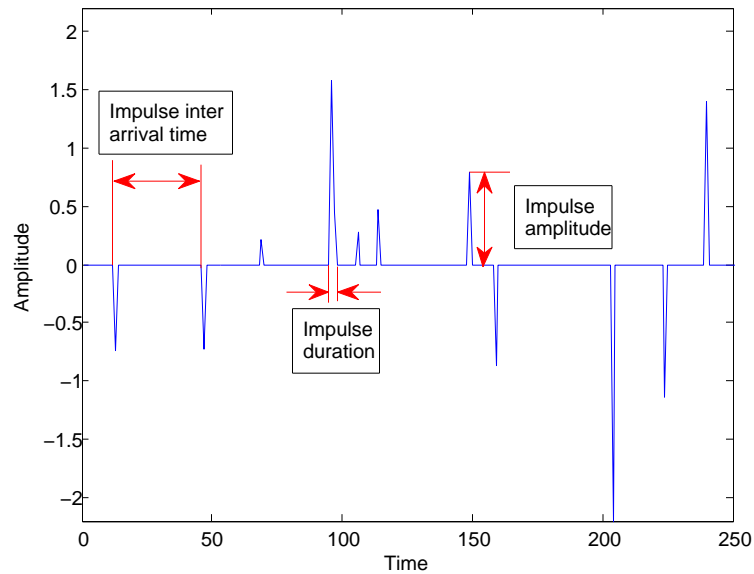


Figure 2.1: Character of Impulsive noise

Impulsive noise is classified into three categories [35]:

1. Class A: Periodic impulsive noise asynchronous with the mains.
2. Class B: Periodic impulsive noise synchronous with the mains.
3. Class C: Asynchronous impulsive noise.

The class A impulsive noise is stationary over time and usually summarized as background noise, while the class B and C are time-variant in term of microseconds to milliseconds. The noise type, discussed in this thesis is classified as class B and C.

2.2.1 Impulsive noise channel models for wireless system

In order to derive impulsive noise characteristics, a mathematical model is needed. I have applied the Bernoulli-Gaussian impulsive noise model of Poisson arriving delta Rayleigh probability density function [36].

The Bernoulli distribution is a discrete probability distribution, which takes value 1 with success probability p , and value 0 with failure probability $q = 1 - p$, with mean p and variance $p(1 - p)$. So if X is a random variable with this distribution, we have:

$$P_r(X = 1) = 1 - P_r(X = 0) = 1 - q = p \quad (2.1)$$

This distribution can be written as

$$X \sim \text{Bern}(p) \quad (2.2)$$

Now if X_1, \dots, X_p are independent, identically distributed (i.i.d) random variables,

then all Bernoulli distributed with success probability p is

$$\sum_{k=1}^n X_k \sim \text{Binomial}(n, p)$$

As we see the Bernoulli distribution is simply Binomial($1, p$).

When signal S is transmitted over a channel with Impulsive Noise In and Additive White Gaussian Noise (AWGN) N , received signal R is described by the following equation.

$$R = S + N + In \quad (2.3)$$

All these parameters are assumed to be complex and independent of each other.

The In is the product of real Bernoulli process b and complex Gaussian process g ,

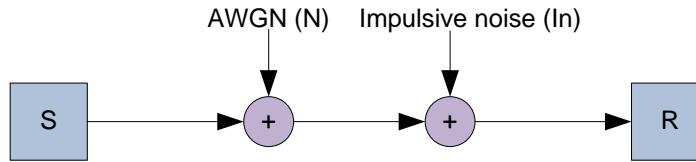


Figure 2.2: Gaussian and impulsive noise channel

also:

$$In = b \cdot g \quad (2.4)$$

This means that each data symbol independently can be hit with the probability of p and with random amplitude g .

The characteristic function (CF) of the Gaussian distribution $\phi_g(\omega_1)$ with mean $\mu = 0$ and variance σ_ω^2 and the CF of the Bernoulli distribution $\phi_b(\omega_2)$ with mean p

and variance $p(1-p)$ are:

$$\phi_g(\omega_1) = e^{-\frac{\sigma_\omega^2 \cdot \omega_1^2}{2}}, \quad \sigma_\omega^2 > 0 \quad (2.5)$$

$$\phi_b(\omega_2) = 1 - p + p \cdot e^{i\omega_2}, \quad 0 < p < 1, p \in \mathbb{R} \quad (2.6)$$

Simply, the product of characteristic function of equation (2.4) is:

$$\phi_{In}(\omega_1, \omega_2) = (1 - p + p \cdot e^{i\omega_2}) \cdot e^{-\frac{\sigma_i^2 \cdot \omega_1^2}{2}} \quad (2.7)$$

With mean zero and variance $\sigma_i^2 = \sigma_\omega^2 \cdot p$.

By definition the Joint characteristic function of two random variable x and y is:

$$\phi_{xy}(\omega_1, \omega_2) = E(e^{i(x\omega_1 + y\omega_2)}) = \int_{-\infty}^{\infty} \int_{-\infty}^{\infty} e^{i(\omega_1 x + \omega_2 y)} f_{xy}(x, y) dx dy \quad (2.8)$$

Hence the characteristic function of the sum of two independent random variables is the product of their characteristic functions [37]. For instance the characteristic function of $z = i + \omega$ with mean $\mu_i = \mu_\omega = 0$ and variances σ_i^2 and σ_ω^2 is:

$$\phi_z(\omega_z) = e^{-\frac{(\sigma_i^2 + \sigma_\omega^2) \cdot \omega_z^2}{2}} \quad (2.9)$$

Thus it can be easily shown that the characteristic function $\Phi(\omega_1 + \omega_2)$ of total noise $Nt = N + In$ of equation (2.3) is:

$$\begin{aligned} \phi_{Nt}(\omega_1, \omega_2) &= (1 - p + p \cdot e^{i\omega_2}) \cdot e^{-\frac{(\sigma_i^2 + \sigma_\omega^2) \cdot \omega_1^2}{2}} = \\ &= (1 - p) \cdot e^{-\frac{(\sigma_i^2 + \sigma_\omega^2) \cdot \omega_1^2}{2}} + p \cdot e^{i\omega_2 - \frac{(\sigma_i^2 + \sigma_\omega^2) \cdot \omega_1^2}{2}} \end{aligned} \quad (2.10)$$

When $p \rightarrow 0$ we get a Gaussian distribution channel, see equation (2.5).

2.3 Conclusions

Manmade noise, particularly impulsive noise, is a main concern in wireless network communications. Therefore, impulsive noise is one significant factor that should always be considered while designing a communication system. In this chapter I presented the characteristic of impulsive noise and a mathematical method for a wireless channel model in the presence of impulsive noise.

Chapter 3

Wireless Two Way Relay Channel system

3.1 Introduction

The purpose of this chapter is to simulate a wireless TWRC system in the presence of impulsive noise and compute the BEP¹ performance of transmitted data. Engineers may use this information to find out an optimal SNR threshold τ^2 for designing an optimal transceiver.

3.2 Network coding

Network coding is a way of relaying packets of information, which are received from different nodes, by combining them together and mapping for broadcasting. The idea of network coding is not new and has existed for more than a decade [38]. The application of network coding has been shown to increase the network throughput.

In general there are two interfaces of network coding:

Digital Network Coding (DNC): Nodes transmit sequentially, relay receives and demodulates signals and then does a linear combination, e.g. XOR-ing, of re-

1. Bit Error Probability

2. The receiver decode received signal if SNR value is above a given threshold τ . Otherwise, it discard signal as an error.

ceived data for broadcasting to respective nodes. It takes 3 time slots. Sometimes the schedule calls for traditional multihop transmissions.

Analogue Network Coding (ANC): Nodes send signals simultaneously to the relay (Multiple Access Channel (MAC) phase), signals combine in the physical channel, called superimposed, and then the relay jointly decodes (map) the superimposed signal. Lastly, the relay re-encodes the signal to an optimized binary signal for broadcasting (Broadcast Channel (BC) phase) to respective nodes [39], Figure 3.1.

The ANC scheme improves the throughput by taking one less time slot as compared to its DNC counterpart. It operates in half duplex mode, but requires strict synchronization [40], [39] in symbol-phase and carrier-frequency between nodes.

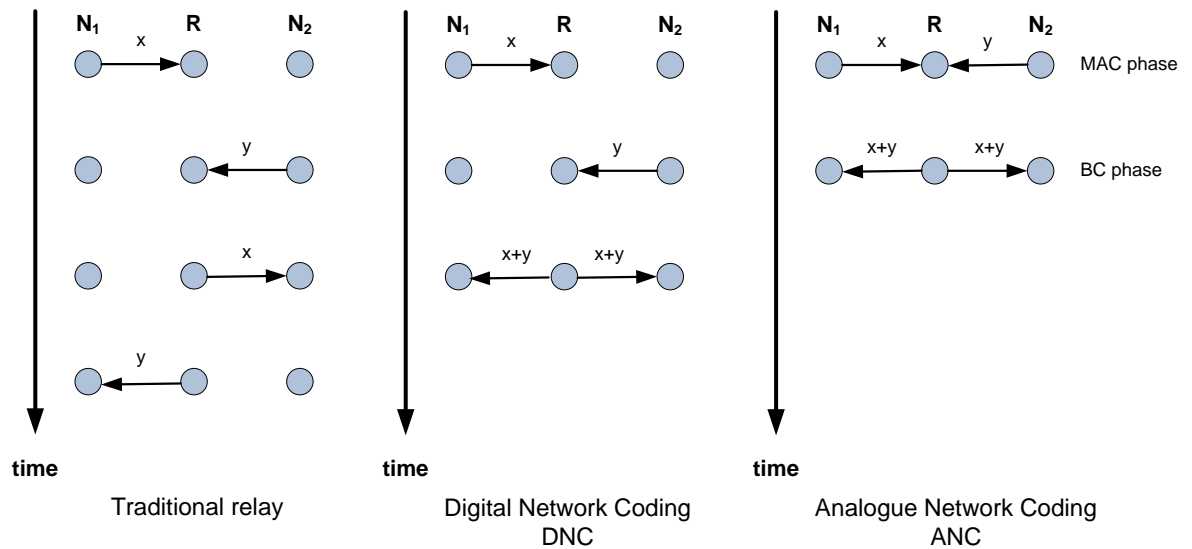


Figure 3.1: Network coding

The network coding interface, discussed in this thesis is analogue network coding.

3.3 System model

Consider a TWRC system with 1 relay node \mathbf{R} and two terminal nodes \mathbf{N}_i , $i = 1, 2$ shown in Figure 3.2, [38].

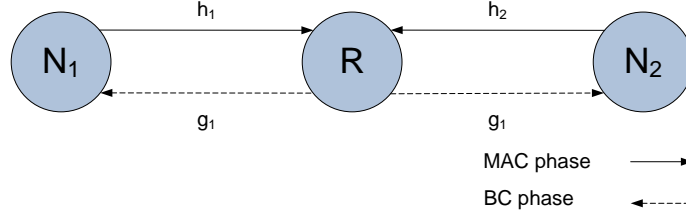


Figure 3.2: System Model for a Two Way Relay Channel

Let S_i denote the message from the source nodes N_i for $i = [1, 2]$, $S_i \sim \mathcal{CN}(0, P)$.

MAC phase

MAC phase means that when N_1 and N_2 simultaneously sent their message signal to the relay R , they respectively are:

$$\begin{aligned} r_1 &= h_1 \sqrt{E_1} S_1(n) + w_r(n) + i_r(n) \\ r_2 &= h_2 \sqrt{E_2} S_2(n) + w_r(n) + i_r(n) \end{aligned} \quad (3.1)$$

where h_1 and h_2 independent complex channel fading coefficient between N_i and R , i.e. $h_i \sim \mathbf{CN}(0, \sigma^2)$. Assume that the channel is unknown to transmitting nodes but perfectly known at receiving nodes. E_1 and E_2 are transmission energies from nodes N_1 and N_2 respectively. $w_r(n)$ is additive white Gaussian noise (AWGN) with mean zero (no dc) and variance σ^2 . $i_r(n)$ is the impulsive noise i.e. Bernoulli-Gaussian process with mean zero and variance $\sigma_\omega^2 \cdot p$, see the equations (2.4), and (2.7).

For simplicity it can be assumed that channel coefficients are constant in two consecutive time slots. It is assumed that the phase of the transmitted signals from N_1 and N_2 are synchronized at the relay node. At the relay these two synchronized

signals add up together $r = r_1 + r_2$ to form a superimposed signal as:

$$r(n) = h_1\sqrt{E_1}S_1(n) + h_2\sqrt{E_2}S_2(n) + w_r(n) + i_r(n) \quad (3.2)$$

Now if the relay amplifies $r(n)$ by a factor β and broadcast $\beta r(n)$ to nodes, the received signal at N_1 is given by

$$\beta r_{s_i}(n) = \beta h_1^2\sqrt{E_1}S_1(n) + \beta h_1 h_2\sqrt{E_2}S_2(n) + \beta h_1 w_r(n) + \beta h_1 i_r(n) + w_r(n) + i_r(n) \quad (3.3)$$

But in the network coding, first the relay detects the received signal, then modulates and broadcasts the detected signal to the nodes. The detection is done by using full channel state information and soft decision decoding. The ML³ detection is given by:

$$d = \min_{S_i} \| y_i - h_1\sqrt{E_1}S_1 - h_2\sqrt{E_2}S_2 \|^2 \quad i = [1, 2] \quad (3.4)$$

The solution for this equation will be uniquely decided, since it is considered that fading channels are totally independent of each other.

The detected signal is mapped by XOR-ed bits from two nodes at the relay.

$$\hat{b}_x = \hat{b}_i \oplus \hat{b}_j \quad i, j = [1, 2] \quad i \neq j \quad (3.5)$$

Broadcast phase

Broadcast means the relay converts back bits b_x into symbols and broadcasts to the

3. Maximum Likelihood

nodes N_1 and N_2 .

$$y_{s_i} = g_i \cdot \sqrt{E_r} X + w_r(n) + i_r(n) \quad i = [1, 2] \quad (3.6)$$

Where, y_{s_i} is the signal sent by the relay to N_1 and N_2 . X is the superimposed symbol message at the relay. g_i , $i = [1, 2]$ are the complex channel gains from the relay to node N_1 and N_2 respectively, and $\sqrt{E_r}$ is the transmission energy at the relay, see Figure 3.2.

By applying the minimum Euclidean distance rule, it follows:

$$d_i = \min_X \| y_{s_i} - g_i \sqrt{E_r} X \|^2 \quad i = [1, 2] \quad (3.7)$$

Finally as the nodes saved their own transmitted signals b_j for $j = [1, 2]$, they simply extracted the transmitted signal from the counterpart node by XOR-ing their own signal from the received signal.

$$\hat{b}_i = \hat{b}_x \oplus b_j \quad i, j = [1, 2] \quad i \neq j \quad (3.8)$$

3.3.1 Error probability analysis

MAC phase

The BPSK modulated signal of N_i will then be $S_i = 2b_i - 1$ where $b_i \in \{0,1\}$ denotes binary information, and $S_i \in \{1,-1\}$ for $i = [1, 2]$ denotes its symbol information. In this system, it is assumed $|h_1| > |h_2|$ that the constellation of the received signal r at relay becomes the same as Figure 3.3, [41].

Where γ is the decision boundary to map $X = 2\hat{b}_x - 1$ which is the symbol information, the relay transmits to both N_1 and N_2 during the broadcast phase.

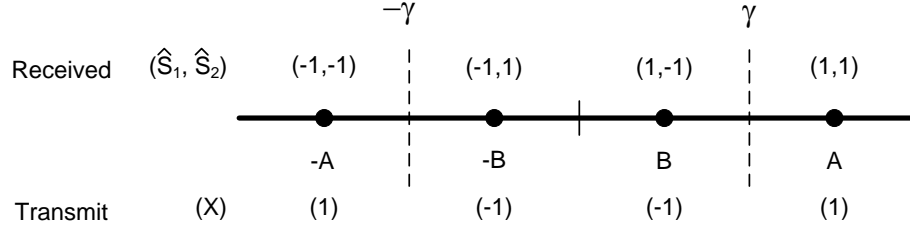


Figure 3.3: Constellation of received signal at the relay node

$$\text{where } A = ||h_1|\sqrt{E_1} + |h_2|\sqrt{E_2}| \\ B = ||h_1|\sqrt{E_1} - |h_2|\sqrt{E_2}|$$

When (S_1, S_2) is equal to $[-1, 1]$ or $[1, -1]$, it will fall into the decision region $[-\gamma, \gamma]$ and hence the relay will transmit -1 towards both sources. Again when (S_1, S_2) is equal to $[1, 1]$ or $[-1, -1]$, it will fall into the decision region outside of $[-\gamma, \gamma]$ and the relay will transmit 1 towards both sources.

To minimize bit errors, the optimal boundary of γ is given by

$$e^{-(\gamma-A)^2/2\sigma_n^2} + e^{-(\gamma+A)^2/2\sigma_n^2} = e^{-(\gamma-B)^2/2\sigma_n^2} + e^{-(\gamma+B)^2/2\sigma_n^2} \quad (3.9)$$

which is equal to

$$\frac{\cosh\left(\frac{\gamma A}{\sigma_n^2}\right)}{\cosh\left(\frac{\gamma B}{\sigma_n^2}\right)} = e^{(A^2-B^2)/2\sigma_n^2} \quad (3.10)$$

For high SNRs where both A and B are greater than $3\sigma_n^2$, the value of γ will approach $\frac{A+B}{2}$ as the decision boundary. The average BEP at the relay P_r for the

MAC phase is written by

$$\begin{aligned}
Pr(\hat{b}_x \neq b_x | y_r(n)) &= E_{\lambda_{min}}[Q(\lambda_{min})] \\
&+ \frac{1}{2} E_{\lambda_{min}, \lambda_{max}}[Q(2\lambda_{max} - \lambda_{min})] \\
&- \frac{1}{2} E_{\lambda_{min}, \lambda_{max}}[Q(2\lambda_{max} + \lambda_{min})]
\end{aligned} \tag{3.11}$$

where

$$\begin{aligned}
\lambda_{min} &= \min \left(|h_1| \sqrt{\frac{2E_1}{2\sigma_n^2}}, |h_2| \sqrt{\frac{2E_2}{2\sigma_n^2}} \right) \\
\lambda_{max} &= \max \left(|h_1| \sqrt{\frac{2E_1}{2\sigma_n^2}}, |h_2| \sqrt{\frac{2E_2}{2\sigma_n^2}} \right)
\end{aligned} \tag{3.12}$$

where $E_x[\cdot]$ denotes the expectation operation over random variable x . By simplify this equation by approximating it with the dominant Q-function⁴ term, we get

$$\begin{aligned}
Pr &\approx E_{\lambda_{min}}[Q(\lambda_{min})] = \frac{1}{2} \times \\
&\left(1 - \sqrt{\frac{E[|h_1|^2] \cdot E[|h_2|^2] \cdot \frac{E_1}{2\sigma_n^2} \cdot \frac{E_2}{2\sigma_n^2}}{E[|h_1|^2] \cdot E[|h_2|^2] \cdot \frac{E_1}{2\sigma_n^2} \cdot \frac{E_2}{2\sigma_n^2} + E[|h_1|^2] \cdot \frac{E_1}{2\sigma_n^2} + E[|h_2|^2] \cdot \frac{E_2}{2\sigma_n^2}}} \right)
\end{aligned} \tag{3.13}$$

4. Q-function is the tail probability of the standard normal distribution.

By applying equation (2.10) for an impulsive channel, we get

$$\begin{aligned}
P_{r_{im}} \approx & \\
(1-p) \cdot \frac{1}{2} \left(1 - \sqrt{\frac{E[|h_1|^2] \cdot E[|h_2|^2] \cdot \gamma_1 \cdot \gamma_2}{E[|h_1|^2] \cdot E[|h_2|^2] \cdot \gamma_1 \cdot \gamma_2 + E[|h_1|^2] \cdot \gamma_1 + E[|h_2|^2] \cdot \gamma_2}} \right) & \\
+p \cdot \frac{1}{2} \left(1 - \sqrt{\frac{E[|h_1|^2] \cdot E[|h_2|^2] \cdot \check{\gamma}_1 \cdot \check{\gamma}_2}{E[|h_1|^2] \cdot E[|h_2|^2] \cdot \check{\gamma}_1 \cdot \check{\gamma}_2 + E[|h_1|^2] \cdot \check{\gamma}_1 + E[|h_2|^2] \cdot \check{\gamma}_2}} \right) & \quad (3.14)
\end{aligned}$$

where $\check{\gamma}_i$, $i = [1, 2]$ is calculated on account of the sum of impulsive SIR⁵ and additive white Gaussian noise SNR, while γ_i , $i = [1, 2]$ is SNR for AWGN for respective channel. p is mean of impulsive noise.

Broadcast phase

The average BEP at the node N_i , $i = [1, 2]$ are given in [42] which are

$$\begin{aligned}
P_{N_i}(\hat{b}_x \neq \hat{b}_x | y_{N_i}(n)) &= E_{h_i} \left[Q \left(|h_i| \sqrt{\frac{2E_r}{2\sigma_n^2}} \right) \right] \\
&= \frac{1}{2} \left(1 - \sqrt{\frac{\frac{E_i}{2\sigma_n^2} \cdot E_r}{2\sigma_n^2 + \frac{E_i}{2\sigma_n^2} \cdot E_r}} \right) \quad i = [1, 2] \quad (3.15)
\end{aligned}$$

Again by applying equation (2.10) for an impulsive channel, we get

$$\begin{aligned}
P_{N_{i_{im}}} &= (1-p) \cdot \frac{1}{2} \left(1 - \sqrt{\frac{\gamma_i \cdot E_r}{2\sigma_n^2 + \gamma_i \cdot E_r}} \right) \\
+p \cdot \frac{1}{2} \left(1 - \sqrt{\frac{\check{\gamma}_i \cdot E_r}{2\sigma_{n+i}^2 + \check{\gamma}_i \cdot E_r}} \right) & \quad i = [1, 2] \quad (3.16)
\end{aligned}$$

End-to-end bit error probability

The end-to-end BEP from node-1 to node-2 is defined as the BEP between the sig-

5. Signal-to-Impulsive-noise Ratio

nal transmitted by node-1 and the signal decoded at node-2 given by

$$\begin{aligned} P_{1 \rightarrow 2} &= P(\hat{b}_1 \neq b_1) = 1 - (1 - P_r)(1 - P_{N_2}) - P_r P_{N_2} = P_r + P_{N_2} - 2P_r P_{N_2} \\ P_{2 \rightarrow 1} &= P(\hat{b}_2 \neq b_2) = P_r + P_{N_1} - 2P_r P_{N_1} \end{aligned} \quad (3.17)$$

Finally, the overall instantaneous end-to-end BEP for the given channel gain is

$$P_{inst} = \frac{1}{2}(P_{1 \rightarrow 2} + P_{2 \rightarrow 1}) \quad (3.18)$$

3.4 Simulations and results

In this section, a performance evaluation will be shown for a wireless TWRC system under a Rayleigh fading conditions with AWGN as well as Impulsive noise environments. The simulation is done by generation of uncorrelated Rayleigh fading sequences by using the simulation software Matlab. The MATLAB random number generator produce normally distributed random numbers. Based on modulation technique and detection method in a loop computes the number of bit errors and bit error rate.

3.4.1 TWRC vs. AF:

In this section, the error rate for TWRC system and the Amplify and Forward (AF) system is measured by varying the value of SNR, while the value of SIR is kept constant.

Figure 3.4 depicts the TWRC system vs. AF system. In the AF system, the relay amplifies the received signal for a factor of β before broadcasting. The amplification

factor β has been chosen as [43]:

$$\beta = \sqrt{\frac{P_R}{|h_1|^2 \cdot P_{N_1} + |h_2|^2 \cdot P_{N_2} + \sigma^2 + p(1-p)}} \quad (3.19)$$

where σ^2 and $p(1-p)$ are AWGN and impulsive noise variance respectively. P_R , P_{N_1} and P_{N_2} are average transmission power at the relay and at the node1 and at the node2 respectively.

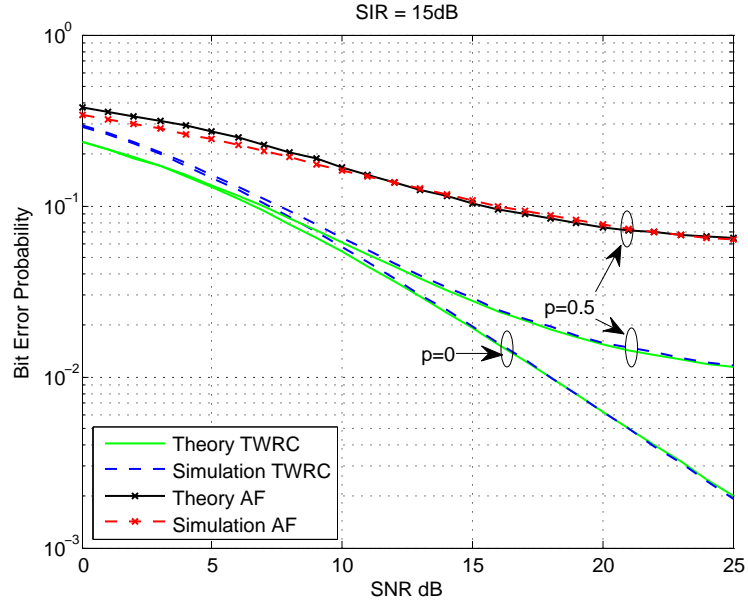


Figure 3.4: TWRC vs. AF relay system

As expected, the TWRC system has higher performance, even when the TWRC is effected by impulsive noise with $SIR=15$ dB and $p=0.5$. This is because of network coding efficiency. The performance curve of the TWRC has more gradual slope than the AF system and less prone to the noise. It can be seen that the simulated BEP performances match the theoretical results provided by equation (3.14) very well.

Basically p is the probability of adding impulsive noise within the system. In other

words, p implies how frequently impulsive noise is added to the received signal. For example, when the value of p is equal to 1, it means that impulsive noise is considered for each bit of the information stream. When p is equal to zero, it indicates that there is no impulsive noise added with the received signal.

3.4.2 BEP as function of SNR

In this section the value of SIR is changed to another value to visualize how the performance changes. For a single value of SIR, different curves are considered by changing the value of p , see Figure 3.5, Figure 3.6 and Figure 3.7.

As expected, when the value of p is increased from 0 to 1, the performance gradually deteriorates. Similarly, when the value of SIR is increased, the performance improves since the strength is increased or, in other words, impulsive noise power is decreased. It is also observed that, while p has a value greater than 0, the graph saturates after a certain value (5 dB to 10 dB). This is happening due to the fact that, although the value of SNR is increasing, which indicates less effect of noise, there is still a certain amount of impulsive noise added to the received signal. Since the increment of SNR does not have any hold on that, the performance curves saturate after a certain SNR value.

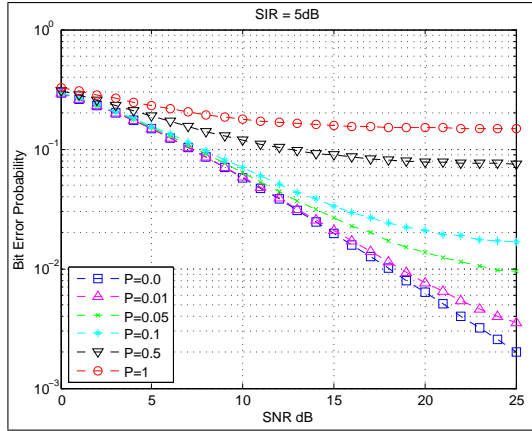


Figure 3.5: TWRC system while SIR=5 dB

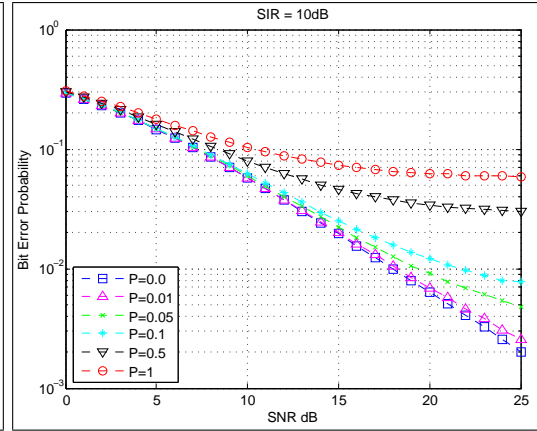


Figure 3.6: TWRC system while SIR=10 dB

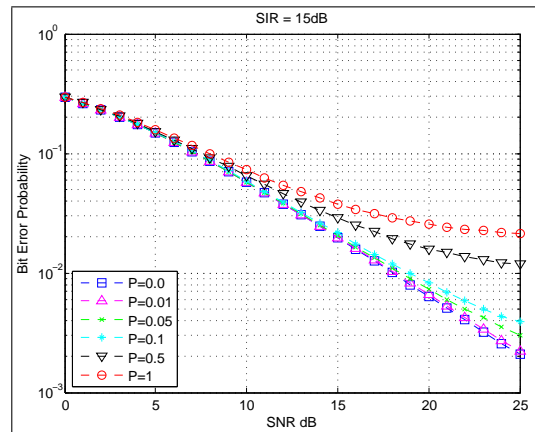


Figure 3.7: TWRC system while SIR=15 dB

3.4.3 BEP as function of SIR

To better analyse the impact of impulsive noise on the system, performance of the TWRC system is studied in this section while varying the value of SIR and fixing the value of SNR. Figure 3.8 shows the average theoretical BEP performances and corresponding curves produced from simulations, which match the theoretical results presented by equation (3.14). One interesting fact can be observed from here. Whenever the value of p is equal to zero, the performance curve is just parallel to the X-axis. When the value of p is zero, it implies that there is no impulsive noise added to the system. In such a case, there is no impact from increasing the value of SIR and the system will only experience a fixed value of AWGN which makes the curve parallel to the X-axis.

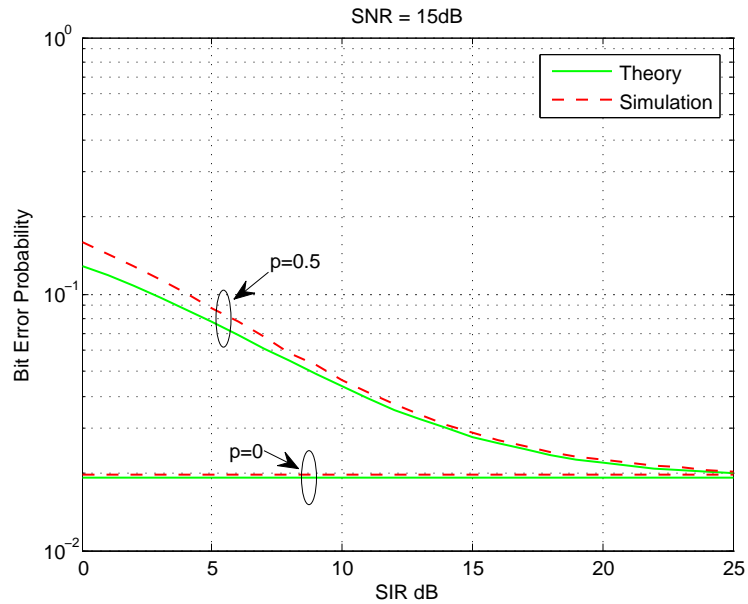


Figure 3.8: TWRC system varying SIR while SNR = 15 dB

Figure 3.9, Figure 3.10 and Figure 3.11 represent the performance graphs for fixed values of SNR as 5 dB, 10 dB and 15 dB respectively, while the SIR is varying.

For each case, the value of p is varied from 0 to 1 which, clearly indicated by the

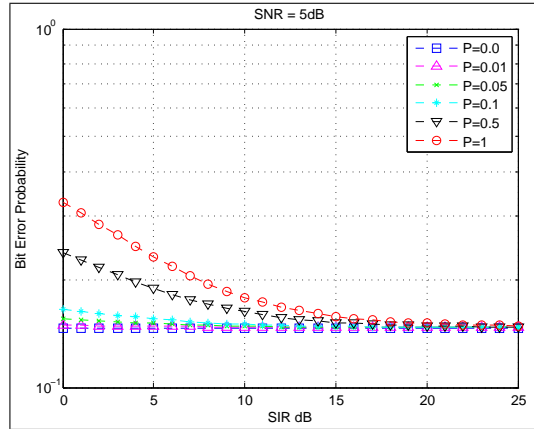


Figure 3.9: TWRC system while SNR=5 dB

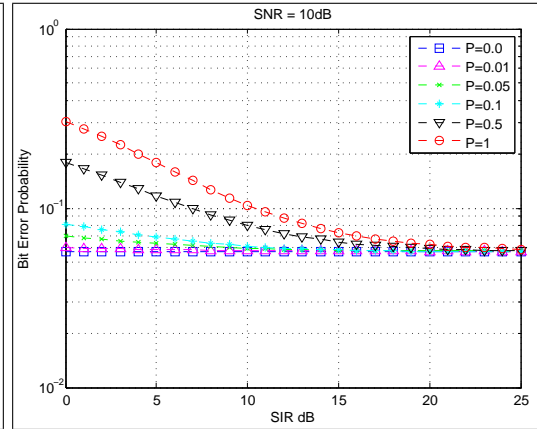


Figure 3.10: TWRC system while SNR=10 dB

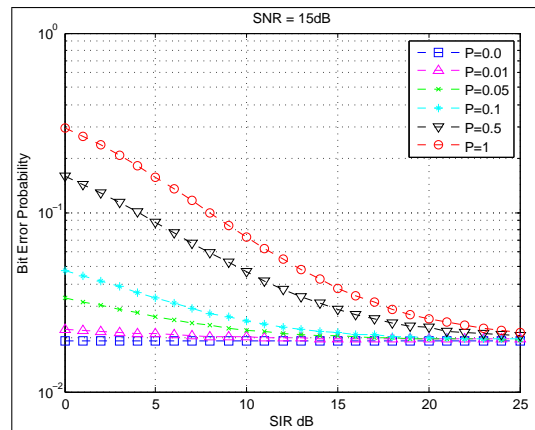


Figure 3.11: TWRC system while SNR=15 dB

figures, shows the value of p is increased, and the performance of the system becomes worse. The saturation effect is similar to the effect described for varying SNR.

3.4.4 BEP as function of SNR and SIR

To more closely study and compare the effect of SIR and SNR, Figure 3.12 illustrates the performance 3D graphs of the TWRC system for a fixed $p = 0.5$, where x, y, and z axis represent SNR, BEP, and SIR respectively. It can be observed that SIR has more deteriorative effect on the system performance than SNR.

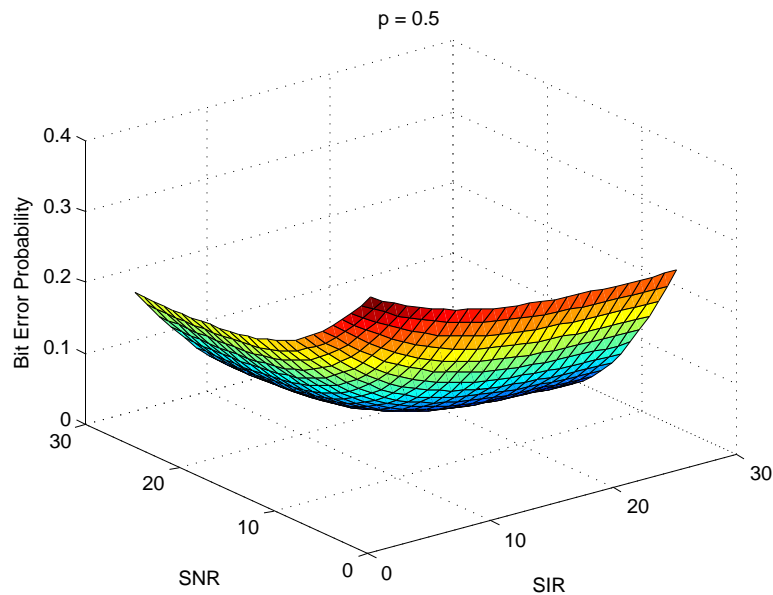


Figure 3.12: TWRC system varying SIR and SNR while $p = 0.5$

The reason is that the impulsive noise has a highly structured form characterized by substantial probabilities of large interference levels and short duration, Figure 2.1 [3]. Therefore the impulsive noise can drastically degrade the performance and the reliability of a wireless communication system even compared with the case of high SNR.

3.4.5 Viterbi decoding algorithm

In this section the error rate is measured by implementing a hard decision decoding Viterbi algorithm⁶ [44] at the relay. I choose the rate for a convolutional encoder 1/2 with a typical generator polynomial $g_1(D) = 1 + D + D^2$ at nodes.

Figure 3.13 represents the performance graphs of the TWRC system with and without the Viterbi decoding algorithm at the relay. The simulation is done for $p=0$ and $p=0.5$. As expected, the system performance increases when I used Viterbi decoding on the relay. Note that the relay performance with Viterbi decoding for $p=0.5$ is even better compared to the relay without Viterbi decoding for $p=0$, particularly for low SNR.

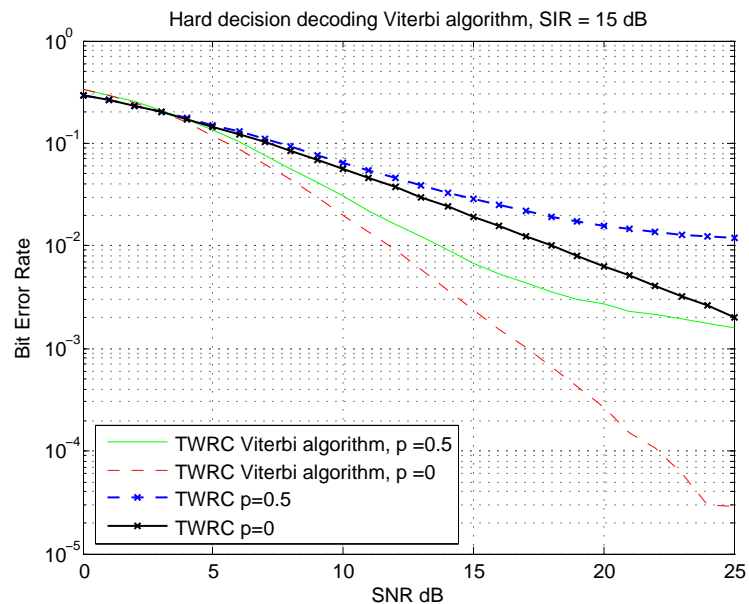


Figure 3.13: TWRC system with the Viterbi decoding

6. The Viterbi algorithm is a ML algorithm for decoding of convolutional codes by choosing a path in the code tree whose codes sequence differs from the received sequence in the fewest number of places.

3.4.6 Adaptive Coding and Modulation

For transmission of high priority data, it is more important to have a reliable link than a higher throughput link. Furthermore sometimes it is advantageous to have a higher throughput link when the channel condition is good and priority is not important. The ACM⁷ can get the information about data priority via coded data in the received signal, and the information about channel condition via Channel State Information (CSI) by using a pilot or embedded pilot symbol in the received signal.

Therefore in this part Asymmetric Modulation (AM) is applied in the TWRC system and performance of the scheme is investigated. I choose a typical case, where one source node uses antipodal BPSK modulation, while the other one uses orthogonal QPSK modulation scheme [45], Figure 3.14. The MAC transmission is the same as the symmetric scenario, but broadcast transmission will be accomplish by two sequenced BPSK transmissions to transfer a QPSK signal from node-2 to node-1. Of course in this phase node-2 will get same signal twice. The relay's constella-

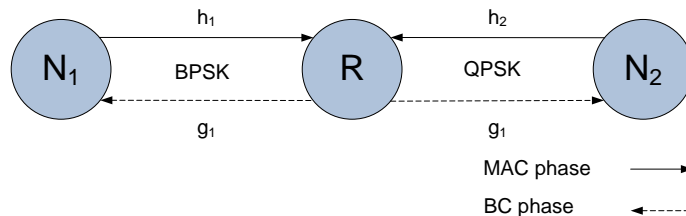


Figure 3.14: An asymmetric TWRC system

tion regions are obtained by calculation of channel gain h_1 and h_2 , which means de-noising mapping will evaluate according to the channel gain. The received signal has 8 ideal normalized constellation points, Figure 3.15.

7. Adaptive Coding and Modulation (ACM) is a technique, which automatically change the modulation depend on priority of data or channel condition.

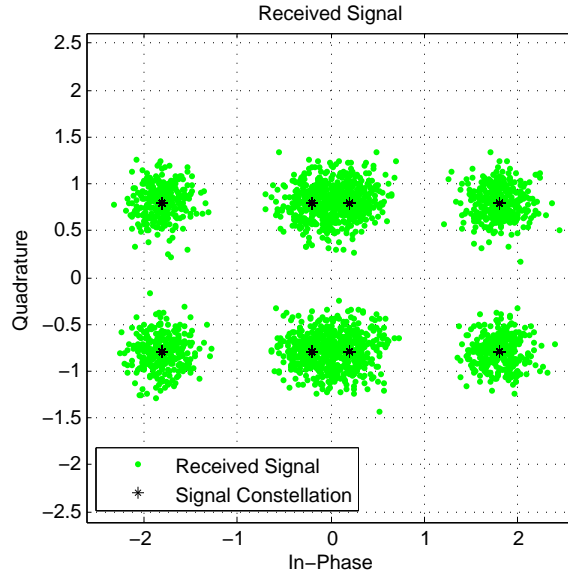


Figure 3.15: Constellation at relay for asymmetric TWRC BPSK and QPSK modulation

In this part, I decided that in all the following steps the relay will amplify the received signal by a factor of β before broadcasting, see equation (3.19). For BPSK modulation at N_1 , symbols is the same as Chapter 3.3.1, but for QAM modulation at N_2 , the symbols will then be $(2b_k - 1) + j(2b_l - 1)$ where $b_k, b_l \in \{0, 1\}$ denotes binary information, and $S_i \in \{\pm 1 \pm j\}$ for $i = [1, 2, 3, 4]$ denotes its symbol information. I assume both channels are affected by Rayleigh fading with AWGN with no impulsive noise environment and with $|h_2| > |h_1|$.

Figure 3.16 represents the performance graphs of the asymmetric modulation of a TWRC system for the relay and both nodes, as well as performance of the symmetric BPSK TWRC system.

The performance of symmetric transmission is better than asymmetric, because the decision boundaries of the asymmetric's Euclidean distance points on constellation are closer to one another compared to the decision boundaries in the symmetric's constellation, see Figure 3.3 and Figure 3.15.

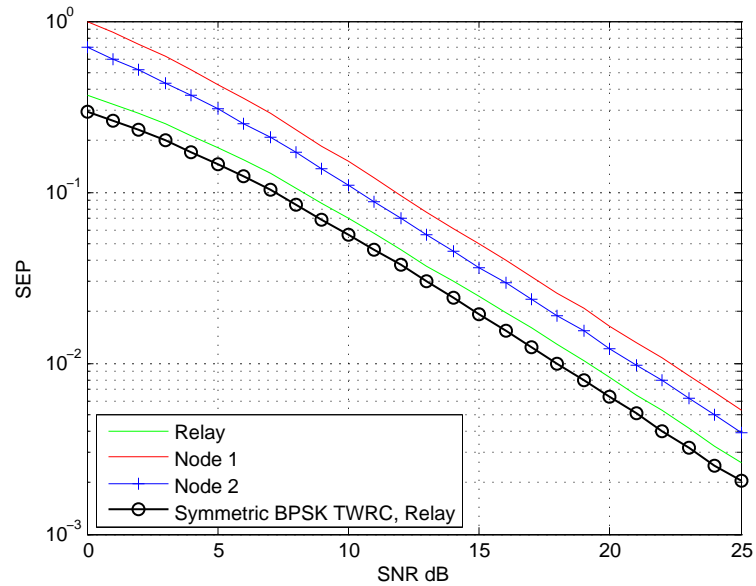


Figure 3.16: Asymmetric modulation of TWRC

For accurate comparison between two nodes, I assumed $|h_1| = |h_2|$, see Figure 3.17. As this figure shows, the BPSK signal received by node-2 has better performance than the QPSK signal received by node-1, and this is because the QPSK signal received from node-2 at the relay should broadcast two sequenced transmissions, which at the end decrease performance of the QPSK symbol compared to the BPSK symbol.

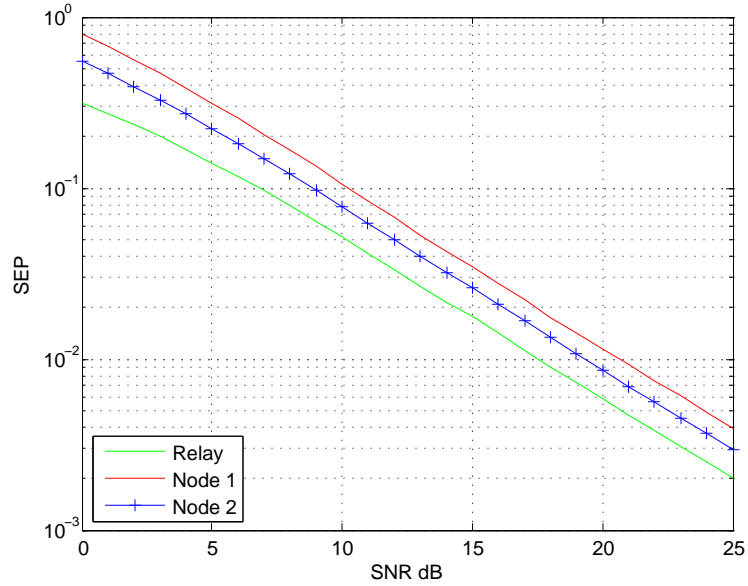


Figure 3.17: Asymmetric modulation of TWRC when $|h_1| = |h_2|$

3.4.6.1 Optimal decision decoding algorithm (ODDA) for asymmetric TWRC

In this section, I will propose an algorithm based on soft decision method for improvement of received signal at one node in a asymmetric TWRC. I name the algorithm Optimal Decision Decoding Algorithm (ODDA).

To present the proposed method, I have used same system as in the previous section, a QPSK and BPSK asymmetric TWRC system. The symbols for BPSK and QPSK modulations are typically given by $S_{iBPSK} = \{\pm 1\}$ and $S_{iQPSK} = \{\pm 1 \pm j\}$ respectively.

As mentioned before, in an asymmetric TWRC system there are two broadcast transmission from the relay in return for one MAC transmission, and the number of sequenced broadcasts depends on the modulation technique. As we know in this example the TWRC system needs two sequenced broadcasts to accomplish a complete transmission.

In conventional TWRC system, received signals at relay after decision and de-noise will be modulated and broadcasted. But in my proposal after decision and de-noise, one of the signals will be formed by XOR-ing of decoded bits of the complex received signal and the other one will be formed the same as the conventional TWRC model. In node-1 after decision, QPSK bits from node-2 will be recovered by XOR-ing. But in node-2, in the first step uses hard decision method to measures Euclidean distance of two sequenced received signals. In the next step decision rules apply to the signal which have least Euclidean distance. This results in decision with the highest probability for received signal, see algorithm 1.

Algorithm 1 Optimal Decision Decoding Algorithm (ODDA) for an asymmetric TWRC

```

MAC
N1 : Sbpsk = ±bi
N2 : Sqpsk = ±bk ± jbl
Air
sum = Sbpsk + Sqpsk
BC
T1 : real(sum) ⊕ imag(sum)
T2 : real(sum)
N2
if distanceT1 > distanceT2 then
    decision = T1 > 0
    b̂i = decision ⊕ bk ⊕ bl
else
    decision = T2 > 0
    b̂i = decision ⊕ bk
end if

```

This method allows the node-2 to detect a limited number of errors that occur anywhere in the signal and correct these errors without retransmission or cost.

It is easy from Figure 3.18 to see that, after the implementation of the optimal decision decoding algorithm, the performance curve of the received signal in node-2 improves. The performance for node-1 remains the same. The same algorithm may

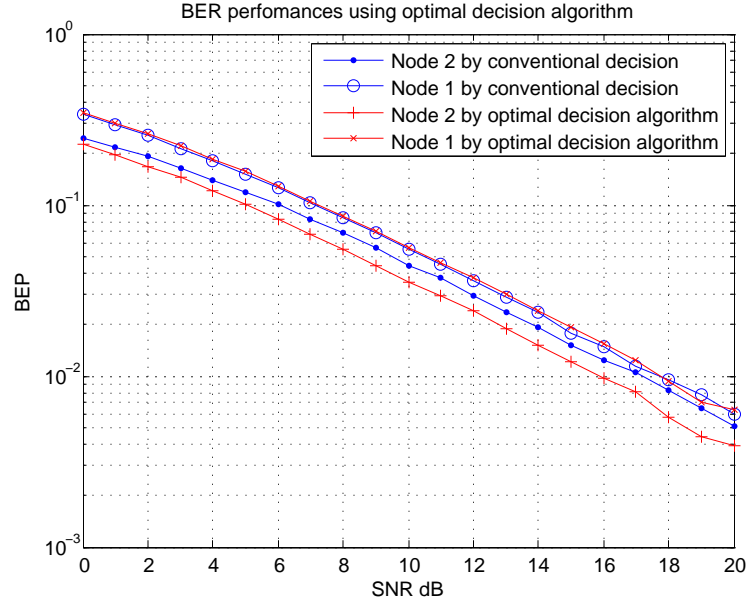


Figure 3.18: Optimal decision decoding algorithm (ODDA) for an asymmetric TWRC

simply apply to higher order modulations in an asymmetric TWRC system.

3.4.6.2 Comparative study of BPSK and QPSK for various signal constellations in a asymmetric TWRC

Finally in this section relays error probabilities studied for various signal constellation types depend on modulation for each node. Simulation have been done for antipodal and orthogonal BPSK and orthogonal and biorthogonal QPSK modulations. I have used the same system as in the previous section.

As Figure 3.19 depicts for cases 1, 3, and 4 the performance of system is almost the same. But in case 2 the performance has decreased, because when both BPSK and QPSK are orthogonal, Euclidean distance points on constellation at relay will have very short distances. This issue may be assumed as a recommendation for the design of any asymmetric TWRC system.

| Case | Node 2 | Node 1 |
|------|--------------------------|------------------------|
| 1 | <i>Orthogonal QPSK</i> | <i>Antipodal BPSK</i> |
| 2 | <i>Orthogonal QPSK</i> | <i>Orthogonal BPSK</i> |
| 3 | <i>Biorthogonal QPSK</i> | <i>Antipodal BPSK</i> |
| 4 | <i>Biorthogonal QPSK</i> | <i>Orthogonal BPSK</i> |

Table 3.1: Case study of constellations types

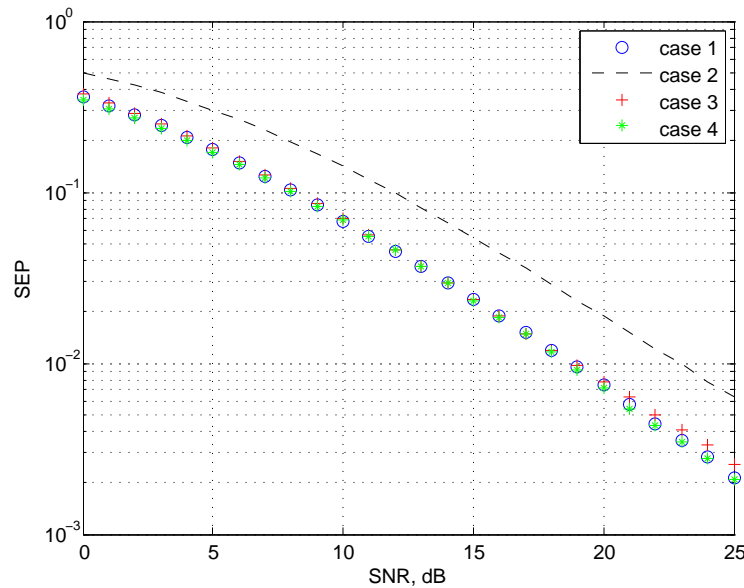


Figure 3.19: Case study of constellation types for an asymmetric TWRC

3.5 Conclusions

Impulsive noise was imposed on the wireless Two Way Relay Channel system for both symmetric and asymmetric systems. The simulation results shows impulsive noise can change the overall performance severely depending upon the intensity of impulsive noise. I used the Viterbi decoding algorithm and a new, which I call Optimal Decision Decoding Algorithm (ODDA) to improve performance and decrease BER for an asymmetric system. The simulation result shows that improvement.

Finally I did a comparative study of BPSK and QPSK for various signal constellations in a asymmetric TWRC system.

Chapter 4

Multi antennas in a wireless TWRC system

4.1 Introduction

In wireless communication, the effect of fading, co-channel interference and error bursts can be combatted using diversity technique via multiple antennas either at the transmitter or receiver. In this section the aim is to analyze the performance of a TWRC system in the impulsive noise environment, that uses multiple antennas at source nodes and the relay.

4.2 System model of Multiple-Input and Single-Output TWRC

The system model of a Multiple-Input and Single-Output (MISO)¹ wireless Two Way Relay Channel (TWRC) 2X1X2 is shown in Figure 4.1. To achieve transmission diversity, Alamouti's space time code [46] is used at the source nodes.

1. Multiple-input and single-output (MISO) when the receiver has a single antenna. Single-input and multiple-output (SIMO) when the transmitter has a single antenna. Multiple-input and multiple-output (MIMO) when the receiver and transmitter has multiple antennas.

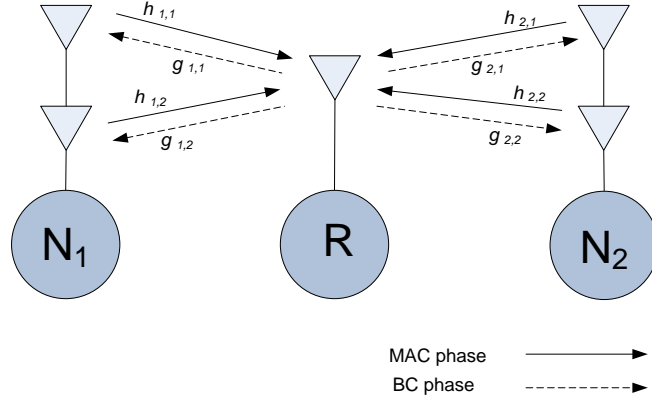


Figure 4.1: A MISO TWRC system

Modulation for the system is BPSK. It is assumed that it is slow fading so that the channel gain $\mathbf{h}_{k,j}$ does not change during two consecutive time slots in each phase for all links. Let k , i , and j denote the indices of source nodes, antennas, and time slots, respectively.

MAC phase

During MAC phase, \mathbf{X} and \mathbf{Y} sent by N_1 and N_2 are as follows:

$$\mathbf{X} = \begin{bmatrix} x_1 & -x_2^* \\ x_2 & x_1^* \end{bmatrix} \quad \text{and} \quad \mathbf{Y} = \begin{bmatrix} y_1 & -y_2^* \\ y_2 & y_1^* \end{bmatrix}$$

respectively. The signal received by relay is:

$$r^T = \sqrt{\frac{E_1}{2}} h_1^T X + \sqrt{\frac{E_2}{2}} h_2^T Y + w^T + i^T \quad (4.1)$$

where $\mathbf{h}_k = \begin{bmatrix} h_{k,1} & h_{k,2} \end{bmatrix}^T$, $k = 1, 2$ is the channel condition of k th channel i.e. the channel from node k of the first or second antenna of that node, E_k is transmitting energy at $Node_k$ and denominator 2 is the number of antenna at $Node_k$.

$w = [w_1, w_2]$ is the AWGN vector at relay node with $w \sim \mathcal{CN}(0, \sigma_R^2 \mathbf{I}_2)$, where \mathbf{I} is an identity matrix with proper size, and at last $i = [i_1, i_2]$ is impulsive noise vector with $i \sim \text{Bern}(p\mathbf{I}_2)$. Assume a slow block fading and perfect channel information at the receiver.

The above transceiver signals can be rearranged as:

$$r = \sqrt{\frac{E_1}{2}} h_1 X + \sqrt{\frac{E_2}{2}} h_2 Y + w + i \quad (4.2)$$

$$\text{where: } \mathbf{r} = \begin{bmatrix} r_1 \\ r_2^* \end{bmatrix}, \mathbf{X} = \begin{bmatrix} x_1 \\ x_2 \end{bmatrix}, \mathbf{Y} = \begin{bmatrix} y_1 \\ y_2 \end{bmatrix}, \mathbf{w} = \begin{bmatrix} w_1 \\ w_2^* \end{bmatrix}, \mathbf{i} = \begin{bmatrix} i_1 \\ i_2^* \end{bmatrix},$$

$$\mathbf{h}_k = \begin{bmatrix} h_{k,1} & h_{k,2} \\ -h_{k,1}^* & h_{k,2}^* \end{bmatrix}, k = 1, 2.$$

Indeed transmitted symbols are recovered by means of simple threshold decoders such as ML or ZF² decoder. In this thesis I have used a ML decoder.

Let s_i denote the symbol vector constructed by the relay by XOR-ing the decoded and demapped superimposed information symbol vectors (x_i, y_i) from the source pair, i.e.,

$$s_i = f(x_i, y_i) = \ell^{-1}((\ell(x_i) + \ell(y_i)) \pmod{M}) \quad (4.3)$$

where $\ell(z) \in 0, 1, \dots, M - 1$ is the label index of z in M , where M is constellation size. The relay has got the CSI of the two channels, which means it knows the modulation used at each user. The maximum likelihood (ML) detection will be employed at the relay according to the received signals from the MAC phase, therefore

2. Zero Forcing refers to a form of linear equalization algorithm used in communication systems which applies the inverse of the frequency response of the channel.

\hat{s}_i can be detected as:

$$\hat{s}_i = \arg \max_{s \in M} \sum_{(X,Y): f(x_i, y_i) = s} \exp(-D(X, Y)) \quad (4.4)$$

where D is the squared Euclidean distance

$$D(X, Y) = \left\| r^T - \left(\sqrt{\frac{E_1}{2}} \cdot h_1^T \cdot X + \sqrt{\frac{E_2}{2}} \cdot h_2^T \cdot Y \right) \right\|^2 \quad (4.5)$$

and E_1 and E_2 are transmission energy at the nodes N_1 and N_2 to R respectively.

Or it can be rewritten as

$$D(X, Y) = \left\| \frac{r^T}{\sigma_R} - \left(\sqrt{\frac{\hat{\gamma}}{2}} \cdot h_1^T \cdot X + \sqrt{\frac{\hat{\gamma}}{2}} \cdot h_2^T \cdot Y \right) \right\|^2 \quad (4.6)$$

where $\hat{\gamma} = E_k/\sigma^2$ is SNR.

Now the network coding will be used to encode the estimated received signals to produce a XOR-ed signal. The XOR-ed signal will be modulate and broadcasted in the next time slot.

BC phase

During the BC phase, the modulated signal is broadcasted to both nodes. The received signal at N_k is:

$$y_{k,j} = \sqrt{E_R} \cdot g_k \cdot \hat{s}_j + w_{k,j} + i_{k,j} \quad j = 1, 2 \quad (4.7)$$

where E_R is the transmit energy at R , $g_k = [g_{k,1} \ g_{k,2}]^T$ is the channel vector of the link from R to N_k , $w_{k,j} \sim \mathcal{CN}(0, \sigma_k^2 \mathbf{I}_2)$ is the AWGN noise vector and $i \sim \text{Bern}(p \mathbf{I}_2)$ is an impulsive noise vector.

The node N_k detects \hat{s}_j as

$$\hat{s}_{k,j} = \arg \min_{s \in M} \| \mathbf{y}_{k,j} - \sqrt{E_{k+2}} \cdot \mathbf{g}_k \cdot \mathbf{s} \|^2 \quad (4.8)$$

where E_{k+2} is transmission energy at the nodes k . Each node detects the symbols sent by the other node by taking the XOR of the detected signal and its own signal:

$$\hat{x}_i = \ell^{-1}((\ell(\hat{s}_1, j) - \ell(y_i)) \pmod{M}) \quad \text{and} \quad (4.9)$$

$$\hat{y}_i = \ell^{-1}((\ell(\hat{s}_2, j) - \ell(x_i)) \pmod{M}) \quad (4.10)$$

where $i = j \in 1, 2$

4.2.1 Error probability analysis

In the system model, \mathbf{g}_k could be modeled to be identical to or independent of \mathbf{h}_k . Basically it depends upon the channels between N_k and R . Let us consider a simple case study that can be quite easily analyzed. I assumed the channel vector \mathbf{g}_k is identical to \mathbf{h}_k for $k = 1, 2$. In addition, for analysis, I assume that $h_{k,i}$, where $k, i \in \{1, 2\}$ and $k \neq i$ are independent and $h_{k,i} \sim \mathcal{CN}(0, 1)$, i.e. Rayleigh fading channels. Let P_m denote the Symbol Error Probability or SEP in the MAC phase for given h_1 and h_2 [47]:

$$P_{mac} \triangleq \frac{1}{2} (P_r\{\hat{s}_1 \neq f(x_1, y_1) | ((\mathbf{X}, \mathbf{Y}), \mathbf{h}_1, \mathbf{h}_2)\} + P_r\{\hat{s}_2 \neq f(x_2, y_2) | ((\mathbf{X}, \mathbf{Y}), \mathbf{h}_1, \mathbf{h}_2)\}). \quad (4.11)$$

In the BC phase $P_{bc,k}$ denotes outage probability at S_k for given h_k :

$$P_{bc,k} \triangleq \frac{1}{2} \sum_{j=1}^2 Pr\{\hat{s}_{k,j} \neq \hat{s}_j | \hat{s}_j, \mathbf{h}_k\}. \quad (4.12)$$

At the relay, in a one-way transmission, if there is only one error in one of two phases, the relay is not able to detect error. But if both the phases have errors, the probability of correct detection is only $\frac{1}{M-1}$, where $M = 2^m$ and $m =$ number of bits. The end-to-end SEP, is given by:

$$P_{EtoE} = P_{mac} + \frac{1}{2} \sum_{k=1}^2 P_{bc,k} - \frac{M}{M-1} P_{mac} \sum_{k=1}^2 P_{bc,k} \quad (4.13)$$

And the average end-to-end SEP is then $\bar{P}_{EtoE} = \mathbb{E}[P_{EtoE}]$, with respect to the distribution of (h_1, h_2) . For my simulation I have BPSK $M = -1, 1$ and $f(x, y) = xy$.

During the BC phase, the upper and lower limits for BPSK, $P_{bc,k}$ is given by

$$P_{bc,k} = \frac{1}{2} \text{erfc}(\sqrt{\tilde{\gamma}_{k+2}} \|\mathbf{h}_k\|) \quad (4.14)$$

During MAC phase, the Alamouti codewords are $\mathbf{X} = [\mathbf{X}_1, \mathbf{X}_2, \mathbf{X}_3, \mathbf{X}_4]$ and $\mathbf{Y} = [\mathbf{Y}_1, \mathbf{Y}_2, \mathbf{Y}_3, \mathbf{Y}_4]$, where $\mathbf{X}_1 = \mathbf{Y}_1 = \begin{bmatrix} 1 & -1 \\ 1 & 1 \end{bmatrix}$, $\mathbf{X}_2 = \mathbf{Y}_2 = \begin{bmatrix} 1 & 1 \\ -1 & 1 \end{bmatrix}$, $\mathbf{X}_3 = \mathbf{Y}_3 = \begin{bmatrix} -1 & 1 \\ -1 & -1 \end{bmatrix}$

$$\mathbf{X}_4 = \mathbf{Y}_4 = \begin{bmatrix} -1 & -1 \\ 1 & -1 \end{bmatrix}$$

Moreover it is very complicated to analyze SEP for the ML detection rule by equation (4.3), since that is a sum of exponential functions. Therefore for ease, a max-log approximation has been applied. The max-log approximation is based on the

assumption that the exponential term with maximum argument in the sum of exponentials will dominate the summation. By avoiding the sum of exponentials only the exponential term remains. The approximation is widely accepted because of its relatively small performance loss.

$$\hat{s}_i = \arg \min_{s \in \{-1,1\}} \min_{(\mathbf{X}, \mathbf{Y}): x_i y_i = s} T(\mathbf{X}, \mathbf{Y}). \quad (4.15)$$

By considering these two mentioned issues, the following calculations derive upper and lower limits for P_{mac} .

4.2.1.1 Upper and lower limits of P_{mac} calculations

To calculate P_{mac} for upper-bound, assume X1 and Y1 is sent, then the XOR-ed-like symbols is $s_1 = s_2 = 1$. Let

$$T_1 = \min_{\substack{(X,Y): x_1 y_1 = 1 \\ (X,Y) \neq (X_1, Y_1)}} T(X, Y);$$

$$T_2 = \min_{(X,Y): x_1 y_1 = -1} T(X, Y)$$

The derivation of error probability for s_1 is:

$$\begin{aligned}
& P_r\{\hat{s}_1 = -1|(X_1, Y_1), h_1, h_2\} \\
&= P_r\{\min(T(X_1, Y_1), T_1) > T_2|(X_1, Y_1)\} \\
&= P_r\{(T_1 \geq T(X_1, Y_1)) \& (T(X_1, Y_1) > T_2)|(X_1, Y_1)\} \\
&+ P_r\{(T(X_1, Y_1) > T_1) \& (T_1 > T_2)|(X_1, Y_1)\} \\
&\leq P_r\{T(X_1, Y_1) > T_2|(X_1, Y_1)\} \\
&+ P_r\{T(X_1, Y_1) > T_1|(X_1, Y_1)\} \\
&\leq \sum_{(m,n) \neq (1,1)} P_r\{T(X_1, Y_1) > T(X_m, Y_m)|(X_1, Y_1)\} \\
&= \sum_{(m,n) \neq (1,1)} P_{PEP,m,n}.
\end{aligned}$$

By doing the same derivation of error probability for s_2 , and combining these equations, the error probability for the upper bound will be determined as:

$$P_{mac}^U \triangleq \sum_{(m,n) \neq (1,1)} P_{PEP,m,n} \quad (4.16)$$

$$P_{PEP,m,n} \triangleq Q(q_{m,n})$$

$$q_{(m,n)} \triangleq \left\| \sqrt{\frac{\bar{\gamma}_2}{4}} h_2^T (X_1 - X_2) \right\|, \quad 1 \leq m, n \leq 4 \quad (4.17)$$

Note that m and n are the indices for codewords.

To calculate P_{mac} for lower-bound, assume that the relay is able to detect X if $\bar{\gamma}_1 \|h_1\|^2 \geq \bar{\gamma}_2 \|h_2\|^2$, or Y otherwise. And if X and Y are known then: $P_{mac} \geq Q(\sqrt{\bar{\gamma}_2} \|h_2\|^2)$ and $P_{mac} \geq Q(\sqrt{\bar{\gamma}_1} \|h_1\|^2)$ respectively, which the lower bounds of P_{mac} resulting as:

$$P_{mac}^L \triangleq Q\left(\sqrt{\min(\bar{\gamma}_1 \|h_1\|^2, \bar{\gamma}_2 \|h_2\|^2)}\right) \quad (4.18)$$

4.2.1.2 Upper and lower limits of end to end error probability calculations

To calculate upper and lower limits for End-to-End error probability, equation (4.13) can be defined as:

$$\begin{aligned}
 \text{Lower bound} &\leq \bar{P}_{EtoE} \leq \text{Upper bound} \\
 \max\left(\mathbb{E}[P_{mac}^L], \frac{1}{2} \sum_{k=1}^2 \mathbb{E}[P_{bc,k}]\right) &\leq \bar{P}_{EtoE} \\
 &\leq \mathbb{E}[P_{mac}^U] + \frac{1}{2} \sum_{k=1}^2 \mathbb{E}[P_{bc,k}]
 \end{aligned} \tag{4.19}$$

For that we need to find $\mathbb{E}[P_{mac}^L]$, $\mathbb{E}[P_{mac}^U]$ and $\mathbb{E}[P_{bc,k}]$.

Because $\|h\|^2$ is chi-square distributed with 4 degrees of freedom, hence $\mathbb{E}[P_{bc,k}] = \phi(2, \bar{\gamma}_{k+2})$ where from [42], equation (14-4-15):

$$\begin{aligned}
 \phi(L, \rho) &\triangleq \left[\frac{1 - \mu(\rho)}{2}\right]^L \sum_{l=0}^{L-1} \left[\frac{1 - \mu(\rho)}{2}\right]^l \\
 \mu(\rho) &\triangleq \sqrt{\frac{\rho}{1 + \rho}}
 \end{aligned} \tag{4.20}$$

Because $(X_1 - X_m)$ and $(Y_1 - Y_m)$ are both orthogonal matrices, we have:

$$q_{m,n} = \sqrt{\bar{\alpha}_{m,n}} \eta_{m,n}^T \tag{4.21}$$

where $\eta_{m,n} = [\eta_{m,n,1}, \eta_{m,n,2}]^T \sim \mathcal{CN}(0, \mathbf{I}_2)$.

The $\bar{\alpha}_{m,n}$ can be found from table 4.1. The value of $\bar{\alpha}_{m,n}$ has been calculated for both the effect of additive white Gaussian noise and the sum of impulsive and additive white Gaussian noise, this later on will be explained in the final calculation of

| $m \setminus n$ | 1 | 2 | 3 | 4 |
|-----------------|-------------------|------------------------------------|-------------------------------------|------------------------------------|
| 1 | – | $\bar{\gamma}_2$ | $2\bar{\gamma}_2$ | $\bar{\gamma}_2$ |
| 2 | $\bar{\gamma}_1$ | $\bar{\gamma}_1 + \bar{\gamma}_2$ | $\bar{\gamma}_1 + 2\bar{\gamma}_2$ | $\bar{\gamma}_1 + \bar{\gamma}_2$ |
| 3 | $2\bar{\gamma}_1$ | $2\bar{\gamma}_1 + \bar{\gamma}_2$ | $2\bar{\gamma}_1 + 2\bar{\gamma}_2$ | $2\bar{\gamma}_1 + \bar{\gamma}_2$ |
| 4 | $\bar{\gamma}_1$ | $\bar{\gamma}_1 + \bar{\gamma}_2$ | $\bar{\gamma}_1 + 2\bar{\gamma}_2$ | $\bar{\gamma}_1 + \bar{\gamma}_2$ |

Table 4.1: Values of $\bar{\alpha}_{m,n}$

P_{EtoE} .

The average PEP is given by $\mathbb{E}[P_{EEP,m,n}] = \phi(2, \frac{1}{2} \cdot \bar{\alpha}_{m,n})$, where the P_{mac}^U from equation (4.16) is given by $P_{mac}^U \triangleq \sum_{(m,n) \neq (1,1)} \phi(2, \frac{1}{2} \cdot \bar{\alpha}_{m,n})$, where $\frac{1}{2}$ is from equation (4.17). Now the upper bound of \bar{P}_{EtoE} can found as:

$$\bar{P}_{EtoE}^U \triangleq \mathbb{E}[P_{mac}^U] + \frac{1}{2} \sum_{k=1}^2 \mathbb{E}[P_{bc,k}] = \sum_{\substack{(m,n) \neq (1,1) \\ 1 \leq m,n \leq 4}} \phi(2, \frac{1}{2} \cdot \bar{\alpha}_{m,n}) + \frac{1}{2} \sum_{k=1}^2 \phi(2, \bar{\gamma}_{k+2}) \quad (4.22)$$

Now if taken into account impulsive noise (equation (2.10)) will give:

$$\begin{aligned} \bar{P}_{EtoE}^U \triangleq & p \left(\sum_{\substack{(m,n) \neq (1,1) \\ 1 \leq m,n \leq 4}} \phi(2, \frac{1}{2} \cdot \bar{\alpha}_{m,n}) + \frac{1}{2} \sum_{k=1}^2 \phi(2, \bar{\gamma}_{k+2}) \right) + \\ & (1-p) \left(\sum_{\substack{(m,n) \neq (1,1) \\ 1 \leq m,n \leq 4}} \phi(2, \frac{1}{2} \cdot \ddot{\alpha}_{m,n}) + \frac{1}{2} \sum_{k=1}^2 \phi(2, \ddot{\gamma}_{k+2}) \right) \end{aligned} \quad (4.23)$$

where $\ddot{\alpha}_{m,n}$ and $\ddot{\gamma}_{k+2}$ are calculated on account of the sum of impulsive and additive white Gaussian noise.

For the lower bound of \bar{P}_{EtoE} , we need to find $\mathbb{E}[P_{mac}^L]$. I assume:

$$\gamma_k = \bar{\gamma}_k \|h_k\|^2, \quad k = 1, 2$$

$$\beta = \min(\gamma_1, \gamma_2)$$

The CDF³ of γ_k is $F_{\gamma_k}(\xi) = 1 - e^{-\frac{\xi}{\bar{\gamma}_k}} - \frac{\xi}{\bar{\gamma}_k} e^{-\frac{\xi}{\bar{\gamma}_k}}$, which yields to the PDF of β as $f_\beta(\xi) = c_1 \xi e^{-\frac{\xi}{\bar{\gamma}_k}} + \frac{c_2}{2\bar{\gamma}} \xi^2 e^{-\frac{\xi}{\bar{\gamma}_k}}$. Hence we will have

$$\begin{aligned} \mathbb{E}[P_{mac}^L] &= c_1 \bar{\gamma}^2 \phi\left(2, \frac{\bar{\gamma}}{2}\right) + c_2 \bar{\gamma}^2 \phi\left(3, \frac{\bar{\gamma}}{2}\right) \\ \text{where } c_1 &\triangleq \frac{1}{\bar{\gamma}_1^2} + \frac{1}{\bar{\gamma}_2^2}, \quad c_2 \triangleq \frac{2}{\bar{\gamma}_1 \bar{\gamma}_1}, \quad \bar{\gamma} \triangleq \frac{\bar{\gamma}_1 \bar{\gamma}_2}{\bar{\gamma}_1 + \bar{\gamma}_2} \end{aligned} \quad (4.24)$$

Now we can find lower bound on \bar{P}_{EtoE}^L by substituting in equation (4.19) as

$$\begin{aligned} \bar{P}_{EtoE}^L &\triangleq \max\left(\mathbb{E}[P_{mac}^L], \frac{1}{2} \sum_{k=1}^2 \mathbb{E}[P_{bc,k}]\right) \\ &= \max\left(c_1 \bar{\gamma}^2 \phi\left(2, \frac{\bar{\gamma}}{2}\right) + c_2 \bar{\gamma}^2 \phi\left(3, \frac{\bar{\gamma}}{2}\right), \frac{1}{2} \phi(2, \bar{\gamma}_3) + \phi(2, \bar{\gamma}_4)\right) \end{aligned} \quad (4.25)$$

Now if taken into account impulsive noise (equation (2.10)) will give:

$$\begin{aligned} \bar{P}_{EtoE}^L &\triangleq p \left(\max\left(c_1 \bar{\gamma}^2 \phi\left(2, \frac{\bar{\gamma}}{2}\right) + c_2 \bar{\gamma}^2 \phi\left(3, \frac{\bar{\gamma}}{2}\right), \frac{1}{2} \phi(2, \bar{\gamma}_3) + \phi(2, \bar{\gamma}_4)\right) \right) + \\ &(1-p) \left(\max\left(c_1 \ddot{\gamma}^2 \phi\left(2, \frac{\ddot{\gamma}}{2}\right) + c_2 \ddot{\gamma}^2 \phi\left(3, \frac{\ddot{\gamma}}{2}\right), \frac{1}{2} \phi(2, \ddot{\gamma}_3) + \phi(2, \ddot{\gamma}_4)\right) \right) \end{aligned} \quad (4.26)$$

where $\ddot{\gamma}$, $\ddot{\gamma}_3$ and $\ddot{\gamma}_4$ are calculated on account of the sum of impulsive and additive white Gaussian noise.

Finally by driving the upper and lower limits for error probability we can prove the simulation of the Alamouti wireless Two Way Relay Channel system.

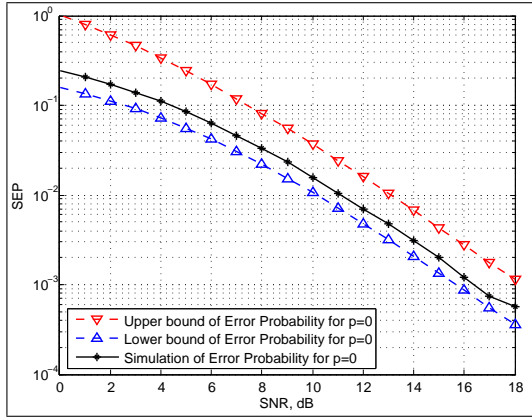


Figure 4.2: Upper and lower bounds when $p = 0$ and $SIR = 10$ dB

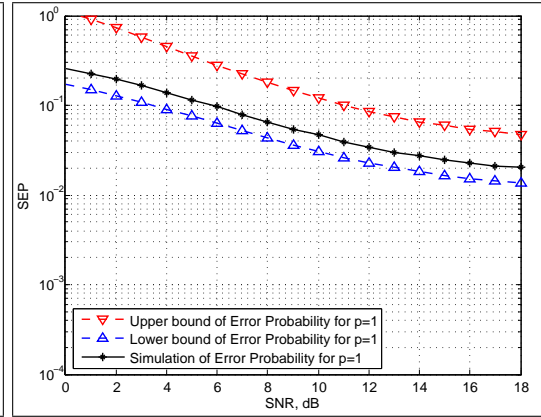


Figure 4.3: Upper and lower bounds when $p = 1$ and $SIR = 10$ dB

4.2.2 Simulations and results

4.2.2.1 SEP as function of SNR

Figures 4.2 and 4.3 show the simulation of SEP while the value of the SIR is kept constant 10 dB for the cases $p = 0$ and $p = 1$. Obviously we see when $p = 1$, the performance of the system deteriorates. The figures also show the upper and lower bounds according to the equations (4.23) and (4.26) respectively. The agreement between the analytical bounds and simulated SEPs for the system shows that derived bounds can predict the performance well. The figure shows that the simulation curve is closer to the lower bound than the upper bounds. The reason is that the approximation in theoretical calculation for the upper-bound result to less accuracy compare to the lower-bound.

4.2.2.2 SEP as function of SIR

In this simulation performance of the system was observed while varying the value of SIR and fixing the value of SNR. Figures 4.4 and 4.5 show clearly the upper and lower bounds according to the equations (4.23) and (4.26) respectively for the cases

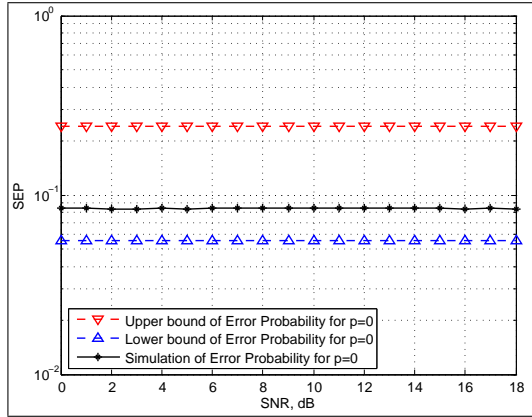


Figure 4.4: Upper and lower bounds when $p = 0$ and SNR = 5 dB

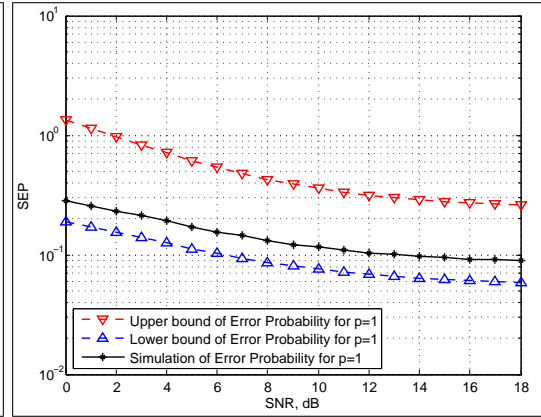


Figure 4.5: Upper and lower bounds when $p = 1$ and SNR = 5 dB

$p = 0$ and $p = 1$. Obviously when $p = 0$, the performance curve is parallel to the X-axis and depends only on the value of SNR, which is fixed. When $p = 1$ the performance of the system becomes worse.

4.2.2.3 Comparison

In this section, the following 3 systems are compared: system-1: the wireless TWRC system described in Chapter 3.3 with and without the presence of impulsive noise, system-2: Alamouti's scheme 2 X 1 without relay and with and without the presence of impulsive noise, and system-3: Alamouti's scheme 2 X 1 with relay and with and without the presence of impulsive noise. For a correct comparison, total transmission power and noise variances are kept equal for each of the systems. The SIR is considered 10 dB for all cases. Obviously the distance between the two nodes

is a double⁴ of that between a source node and the relay in system-2.

Figure 4.6 shows obviously that system-3 performance is better than system-1 because of higher diversity gain at system-3. In addition the Alamouti schemas outperforms single antenna relay as well when the impulsive noise is high. As the Fig-

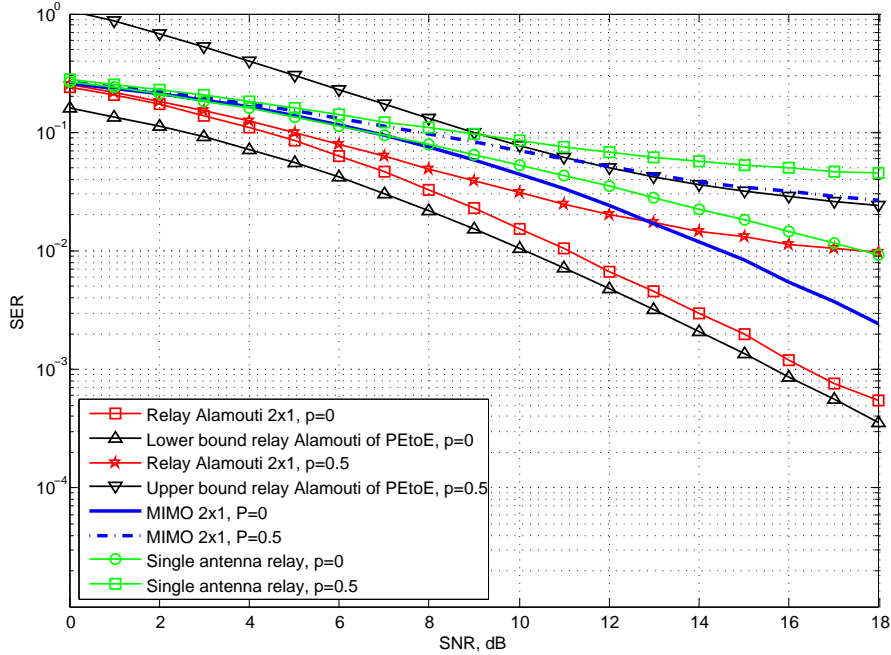


Figure 4.6: Performance comparison of different systems, SIR = 10 dB

ure shows system-3 performs better than system-2 since in system-3 the relay de-noise and forward signals, while in system-2 the relay just transfers signals directly. It is interesting to note that the system-2 performance is better than the system-1 performance.

4. Let the transmitted signal power be P_t , and the received power be P_r . Let the frequency denoted by f , and c be the speed of light. The distance between the transmitter and receiver is D . Let G_t and G_r represent the transmitter and receiver antenna gains respectively. The upper limit of the power received, when power P_t is transmitted is given by the Friis formula, which accounts for the free space path loss $P_r = P_t G_t G_r \left(\frac{c}{4\pi D f} \right)^2$. The Friis free space formula shows that the received power falls off as the square of the transmitter-receiver distances.

4.3 System model of Multiple-Input and Multiple-Output TWRC

The system model of a Multiple-Input and Multiple-Output (MIMO) wireless Two Way Relay Channel (TWRC) 2X2 is shown in Figure 4.7 [48]. In this system the

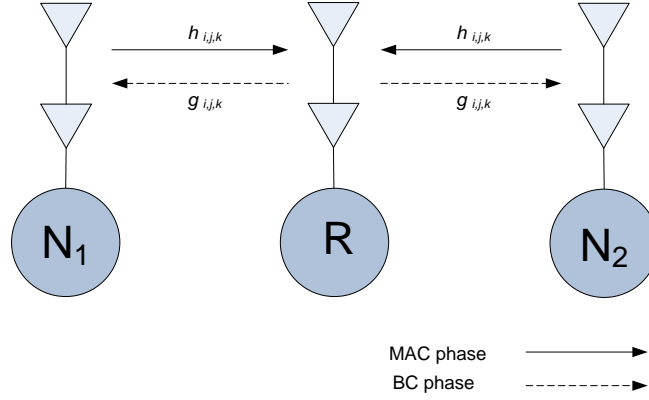


Figure 4.7: A MIMO TWRC system

nodes and the relay are each equipped with two antennas to improve the transmission quality. Let $x_{i,j}$, $i, j = \{1, 2\}$ denote the symbol transmitted by the j th antenna of node N_i , $i = \{1, 2\}$, which is represented by matrix X_i . The received symbol matrix Y_r at the relay can be written as

$$Y_r = \sqrt{\frac{E_1}{A_{N_1}}} H_1 X_1 + \sqrt{\frac{E_2}{A_{N_2}}} H_2 X_2 + W_r + I_r \quad (4.27)$$

where H_i is the fading channel coefficient matrix with elements $h_{i,j,k}$, from node N_i 's j th antenna to the relay's k th antenna, and W_r and I_r are the AWGN and impulsive noise matrix respectively at the relay's j th antenna. A_{N_i} is the number of antennas at node N_i , which in our case is 2, and E_i is transmitting energy at node N_i .

The relay decodes the received symbol using ML decision to obtain $\hat{x}_{i,j}$. After network coding we get $\hat{\hat{x}}_{i,j}$, which the relay after modulation broadcasts to both nodes. Thus at the broadcast phase, node N_i receives

$$Y_i = \sqrt{\frac{E_r}{A_R}} G_i \hat{\hat{X}}_i + W_i + I_i \quad (4.28)$$

where Y_i receives the signal matrix at node N_i , and G_i is the fading channel coefficient matrix with elements $g_{i,j,k}$, from the relay's k th antenna to the node N_i 's j th antenna. A_R is the number of antennas at the relay, which in our case is 2, and E_r is transmitting energy at the relay.

Finally the nodes N_i perform ML decoding and extracts transmitted symbols from the other terminal with its own symbols.

4.3.1 Simulations and results

In the simulation, I assumed that the perfect CSI is available for all nodes and the relay. I did a simulation for a MIMO TWRC 2x2 system and compared it with the result from the previous section, namely a MISO TWRC 2x1 system. Figure 4.8 shows obviously that MIMO TWRC performance is almost 3 dB better than MISO TWRC because of higher diversity gain at the relay.

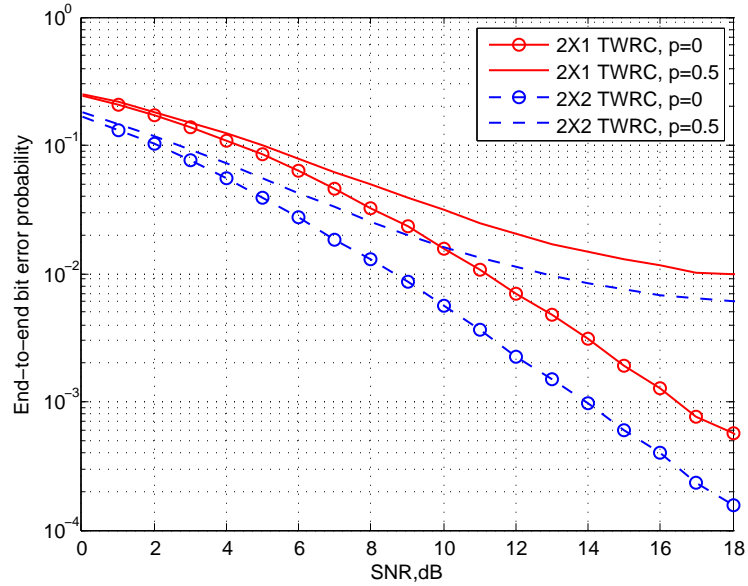


Figure 4.8: MIMO TWRC system vs. MISO TWRC system

4.4 Conclusions

By using multiple antennas at both the transmitter and receiver we can improve communication performance. This improvement is achieved by higher spectral efficiency, more bits per second per hertz of bandwidth, and link reliability or diversity. In this chapter I analyzed the performance of a TWRC MISO system in an impulsive noise environment by using multiple antennas at the source nodes while using a single antenna at the relay node with Alamouti schemes. I compared the results with a single antenna TWRC system. Finally I analyzed the performance of a MIMO TWRC system and compared its performance with a TWRC MISO system.

Part II

Polarization

Chapter 5

Polarized antennas in a wireless TWRC system

5.1 Introduction

The next generation wireless TWRC system will demand high data rate services to meet requirements from various applications [49]. In this chapter, I propose a new TWRC scheme based on polarization, which is able to transmit and receive data between nodes simultaneously, in other words full duplex system, by using the same carrier frequency.

5.2 Polarized Antenna Network Coding (PANC) and full duplex PANC

Until now the half duplex wireless TWRC system has been analyzed, which suffers from time delay, since relay nodes have to wait until adjacent nodes complete their transmission, because in the time domain there is only one channel for transmission. This also affects the spectral efficiency, because in the time domain, half of data transmission capacity is available in both directions.

One way to address these issues is by having two channel resources, one for the first hop (source to relay) and another for the second hop (relay to destination). Hence

the number of channel resources get doubled, since the available spectrum is scarce and expensive. It is not a good approach. The other disadvantage to having two carrier frequencies is related to the synchronization issue that exists between the relay and the nodes, which increase complexity of the system synchronization.

However here I propose a new scheme to achieve a full duplex transmission system and decrease transmission delay, while using the same carrier frequency, which I call Full duplex Polarized Antenna Network Coding (PANC), Figure 5.1.

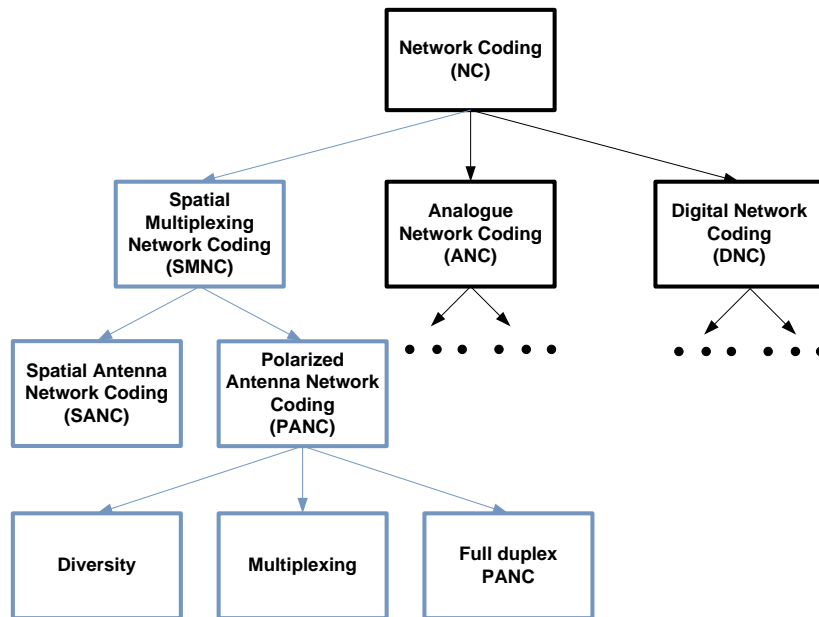


Figure 5.1: Network coding

Horizontal, vertical, left- and right-hand circular polarized transmissions will not interfere with each other, because they are differently polarized. This means signals via same carrier frequency can be transmitted and received simultaneously by different polarizations via a transceiver.

To this end consider a wireless TWRC system with two nodes and one relay, each

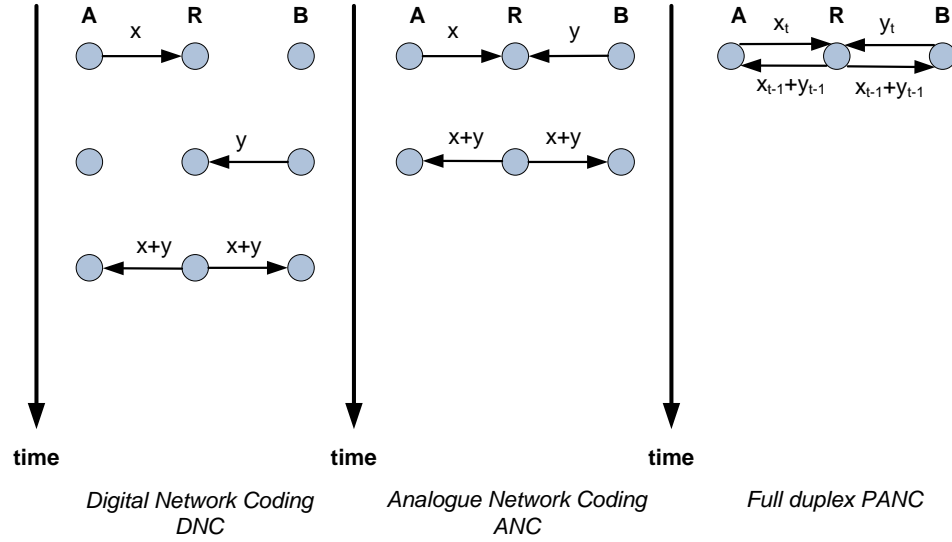


Figure 5.2: Network coding as function of time

one with a linear cross-polarized antenna, e.g. vertical and horizontal polarized¹.

The relay station initially in the first time slot receives the XOR-ed signal from two nodes. It jointly decodes the superimposed signal, re-encodes it, and in the second time slot relay sends the signal back to respective nodes while it receives the next XOR-ed signal, Figure 5.2.

It is the same scenario for nodes. In the second time slot they receive the relay signal while sending the next signal. During the second time slot the nodes cancel the self interference (XOR with own signal) from the received relay signal and get the useful data. This reduces one time slot and saves one channel resource, which improves spectral efficiency or throughput by one time slot as compared to a conventional ANC. Note that although we are dealing with one physical cross-polarized transceiver antenna (+), the underlying channel is a 2-input 2-output channel, since

1. Note the antennas polarization is distinguished as co-polarized (||), dual-polarized (|-) or cross-polarized (+) [50].

each polarization mode is treated as an independent physical channel.

5.3 System model

The idea behind polarized channel modeling is to determine how much the wave components are related in the polarization plan and to determine how this effects the communication system.

Transmitter: When signal $x(t)$ is transmitted by an antenna, which have both electrical fields \vec{E}_θ and \vec{E}_ϕ polarizations, the free space radiated far field will be [51]

$$\begin{bmatrix} E_\theta(\theta, \phi, t) \\ E_\phi(\theta, \phi, t) \end{bmatrix} = \frac{e^{-j\vec{k}\cdot\vec{d}}}{d} \begin{bmatrix} h_\phi(\phi, \theta) \\ h_\theta(\phi, \theta) \end{bmatrix} x(t) \quad (5.1)$$

where d is the distance from the antenna. The antenna's mismatch, efficiency, etc. is represented by h vector [50].

Receiver: The receive signal $y(t)$ on the receiver antennas in the free space without scatters is given by:

$$y(t) = [h_\phi^r(\phi_r, \theta_r) \ h_\theta^r(\phi_r, \theta_r)] \frac{e^{-j\vec{k}\cdot\vec{d}}}{d} \begin{bmatrix} h_\phi^t(\phi_t, \theta_t) \\ h_\theta^t(\phi_t, \theta_t) \end{bmatrix} x(t) = \frac{e^{-j\vec{k}\cdot\vec{d}}}{d} x(t) (h_\theta^r(\theta_r, \phi_r)h_\theta^t(\theta_t, \phi_t) + h_\phi^r(\theta_r, \phi_r)h_\phi^t(\phi_t, \theta_t)) \quad (5.2)$$

where (θ_t, ϕ_t) are the angles of the wave at the transmitter, and (θ_r, ϕ_r) are the angles of the wave at the receiver, and $x(t)$ is the transmitted signal, d is the distance between the transmitter and receiver, and h^t and h^r are the radiation patterns of the transmit and receive antenna, respectively.

Now if we assume scatters, which will change the polarized wave as shown in Figure 5.3 this will result as transmitted signal:

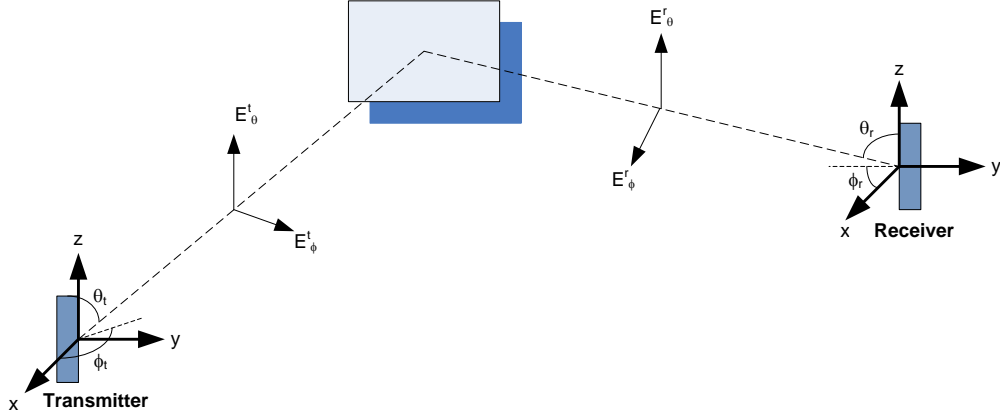


Figure 5.3: Polarized wave and scatter

$$\begin{bmatrix} E_{\theta}^r \\ E_{\phi}^r \end{bmatrix} = \begin{bmatrix} \gamma_{\theta\theta} & \gamma_{\theta\phi} \\ \gamma_{\phi\theta} & \gamma_{\phi\phi} \end{bmatrix} \begin{bmatrix} E_{\theta}^t \\ h_{\phi}^t \end{bmatrix} \quad (5.3)$$

where E_{ϕ}^t and E_{θ}^t are the polarization components of transmitted signal and E_{ϕ}^r and E_{θ}^r are the polarization components of the arrived signal. The terms of matrix γ are path losses due to the interaction.

Adding scatters component to the equation (5.2) for the receiver give:

$$y(t) = [h_{\phi}^r(\phi_r, \theta_r) \ h_{\theta}^r(\phi_r, \theta_r)] \begin{bmatrix} \gamma_{\theta\theta} & \gamma_{\theta\phi} \\ \gamma_{\phi\theta} & \gamma_{\phi\phi} \end{bmatrix} \frac{e^{-j\vec{k} \cdot \vec{d}}}{d} \begin{bmatrix} h_{\phi}^t(\phi_t, \theta_t) \\ h_{\theta}^t(\phi_t, \theta_t) \end{bmatrix} x(t) \quad (5.4)$$

To convey the idea of a channel model for a dual-polarized transceiver antenna, assume that the channel is frequency-flat. Then the signal model is given by:

$$r = \sqrt{E} \cdot H_t \cdot s + n \quad (5.5)$$

where the r is received signal vector, the \sqrt{E} is average energy at each transmitter antenna for every symbol average. The H_t is the total channel polarization matrix. The s is the signal vector with normalized average energy, and n is the noise vector with i.i.d. zero-mean complex Gaussian. The dimension of s and obviously H_t and n depends on the number of transmitter polarized antennas. It is possible to add non Gaussian noise here too, as I did in Chapter 3.3 for impulsive noise.

The channel polarization matrix H_t , represents co and cross-polarized components, cross-correlation and cross-coupling of energy from one polarization mode (vertical/horizontal $0^\circ/90^\circ$ or slanted $+45^\circ/-45^\circ$) to the other polarization mode. The wireless TWRC system are immobile, so it means a fixed part of multipath signal components will not change for different channel time samples, but a small part of the multipath signal components will vary due to the movements of the environments. Therefore the channel polarization matrix H_t decomposed into the sum of the fixed (line-of-sight) part and the average random (fast fading) part.

$$H_t = \underbrace{\sqrt{\frac{K}{1+K}} \bar{H}_{n \times m}}_{\text{Fixed part}} + \underbrace{\sqrt{\frac{1}{1+K}} \tilde{H}_{n \times m}}_{\text{Variable part}} \quad (5.6)$$

Where K is the Rician K-factor, and $\bar{H}_{n \times m}$ is a deterministic or time-static channel matrix, which received a contribution from Line Of Sight (LOS), and $\tilde{H}_{n \times m}$ is a random or time-variant channel matrix which received a contribution from Non Line Of Sight (NLOS) for an n-receiver m-transmitter (MIMO) system. Hence if $K = 0$ then H_t will represent a Rayleigh fading channel and if $K \rightarrow \infty$ it will represent a static channel [52], [53].

The Friis free-space equation shows that the received power falls off as the square of the transmitter-receiver distance d , along with Malu's law for polarized wave,

which shows that received power is directly proportional to the square of the cosine of polarization mismatch angle θ between the polarized incident wave on the receiver antenna and angle of polarized antenna with respect to angle of polarization direction of the wave, and finally along with snell's law of reflection [54], [55], gives the total received power result of the line-of-sight component and non-line-of-sight component as:

$$P_R = \left(\frac{\lambda}{4\pi}\right)^2 G_R G_T P_T \left| \underbrace{C_{pol}(\theta) \frac{e^{-jkd_1}}{d_1}}_{line-of-sight} + \underbrace{C_{ref}(\phi) \frac{e^{-jkd_2}}{d_2}}_{non-line-of-sight} \right|^2 \quad (5.7)$$

where $k = 2\pi/\lambda$ is the free-space wavenumber, d_1 is the distance between transmitter and receiver for line-of-sight path, and $d_2 = d_{2t} + d_{2r}$ is the total path for non-line-of-sight.

C_{pol} is the polarization mismatch component including azimuthal displacement of the transmit and receive antenna (The azimuthal displacement only has effect on a horizontal oriented antenna). C_{ref} is the reflection component for non-line-of-sight case. G_T and G_R are transmitting and receiving antenna gain respectively. P_T and P_R are transmitted and received power respectively. The model has shown in Figure 5.4, where the earth assumed to be flat.

Now if we are assuming that the transmitter and receiver antenna consists of n pairs and m pairs of cross-polarized, vertical(V) and horizontal(H), antennas respectively, the channel matrix for LOS and NLOS component can be written as:

$$\bar{H}_{LOS} = \begin{bmatrix} \bar{H}_{n \times m}^{VV} & \bar{H}_{n \times m}^{VH} \cdot A_z \\ \bar{H}_{n \times m}^{HV} & \bar{H}_{n \times m}^{HH} \cdot A_z \end{bmatrix} \quad (5.8)$$

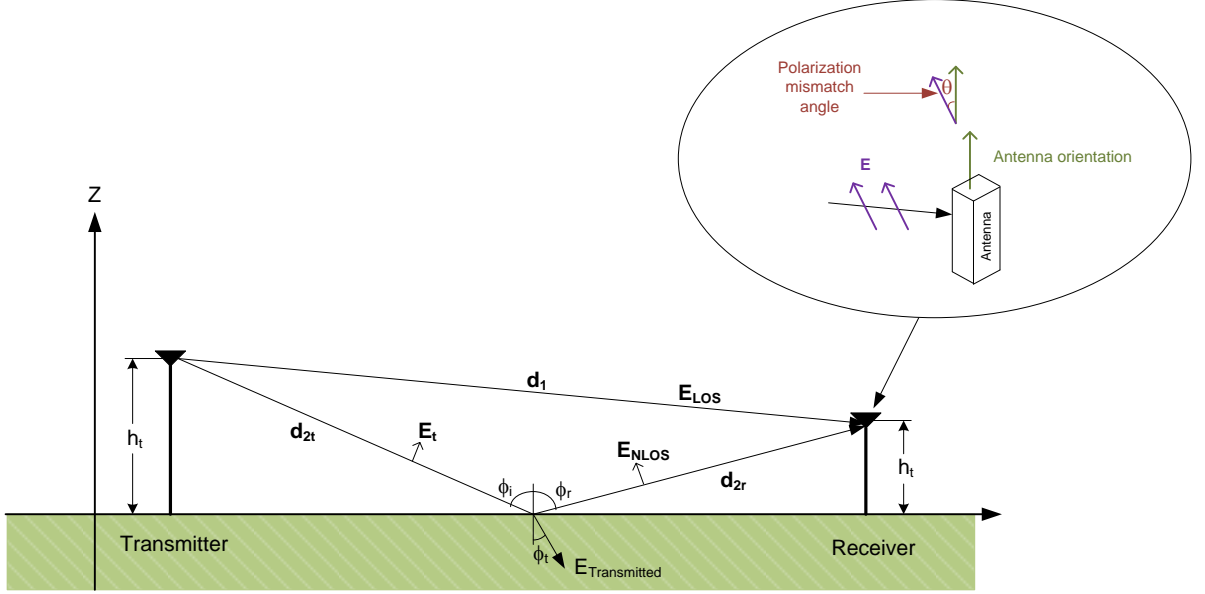


Figure 5.4: Geometry for the two-ray propagation model

$$\tilde{H}_{NLOS} = \begin{bmatrix} \tilde{H}_{n \times m}^{VV} & \tilde{H}_{n \times m}^{VH} \cdot A_z \\ \tilde{H}_{n \times m}^{HV} & \tilde{H}_{n \times m}^{HH} \cdot A_z \end{bmatrix} \quad (5.9)$$

For line-of-sight the elements of matrix $\tilde{H}_{n \times m}^{xy}$ ($x, y = V, H$) can be obtained according to Malu's law:

$$\bar{h} = \frac{e^{-jkd_1}}{d_1} G_R G_T \cdot \cos\theta_r \quad (5.10)$$

where $\cos\theta_r$ is the polarization mismatch component (equation (5.7)) and θ_r is the polarization mismatch rotation angle between the transmitter and receiver. If the transmitter and receiver are all strictly aligned, namely co-polarized, then θ_r is equal to 0 for the channel between VV and HH, while θ_r is equal to $\pi/2$ for the channel between HV and VH, namely orthogonally oriented. But in reality the transmitter and the receiver antenna are not aligned because if the polarization mismatch component for VV and HH channel is $\cos\theta_r$ then for VH and HV polarization mismatch becomes $\cos(\pi/2 - \theta_r)$. So the channel components for LOS

are:

$$\begin{aligned}\bar{h}^{x,x} &= \frac{e^{-jkd_1}}{d_1} G_R^x G_T^x \cdot \cos\theta_r, & x = V, H \\ \bar{h}^{x,y} &= \frac{e^{-jkd_1}}{d_1} G_R^x G_T^y \cdot \cos(\pi/2 - \theta_r), & x, y = V, H\end{aligned}\quad (5.11)$$

The A_z in the equations (5.8) and (5.9) is azimuthal displacement of the transmitter and receiver antennas for horizontally polarized transmitting signals, and if we assume that the angle of arrival at the receiver is ψ^A and the angle of departure at the transmitter is ψ^D , then $A_z = \cos\psi^A \cdot \cos\psi^D$.

For non-line-of-sight, the element of matrix $\tilde{H}_{n \times m}^{xy}$ ($x, y = V, H$) can be obtained according to snell's law:

$$\begin{aligned}\tilde{h}^{x,x} &= \sum_{i=1}^{ns} \frac{e^{-jkd_{2,i}}}{d_{2,i}} G_{R,i}^x G_{T,i}^x \cdot \alpha_i(\phi_i) \cdot \cos\theta_{r,i}, & x = V, H \\ \tilde{h}^{x,y} &= \sum_{i=1}^{ns} \frac{e^{-jkd_{2,i}}}{d_{2,i}} G_{R,i}^x G_{T,i}^y \cdot \alpha_i(\phi_i) \cdot \cos(\pi/2 - \theta_{r,i}), & x, y = V, H \\ \Rightarrow \lim_{ns \rightarrow \infty} &\simeq \sqrt{P_r^{NLOS}} \begin{bmatrix} h_{vv} & h_{vh} \\ h_{hv} & h_{hh} \end{bmatrix}\end{aligned}\quad (5.12)$$

where $\alpha_i(\phi_i)$ is the reflection components (equation (5.7)) which describes the total amplitude and phase changes due to the reflection, diffraction and scattering on propagation paths. The ns is the number of paths, in other words, \tilde{H}_{NLOS} is the summation of all multipath field components for transmitter and receiver antenna pairs, which according to the central limit theorem can be approximated as i.i.d. Gaussian model. When ns is big enough, the channel may be approximated by the Rayleigh channel, where P_r^{NLOS} is the total received power, h_{vv}, h_{hh}, h_{vh} and h_{hv} are i.i.d. complex Gaussian random variables.

Channel XPD : As mentioned above, the electromagnetic wave due to reflection, diffraction or scattering changes its polarization mode through a channel. The channel cross-polarization discrimination XPD describes a channel that has a symmetric leakage from one polarization mode V/H to another polarization mode V/H, in other words, the XPD represents the channel's ability to separate V and H polarization, Figure 5.5.

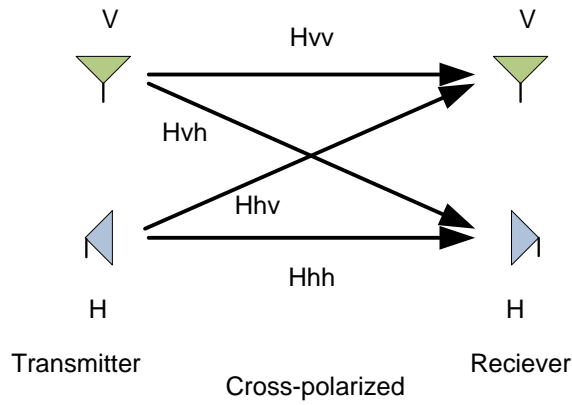


Figure 5.5: A cross-polarized channel

The XPD defined as:

$$XPD^V = \frac{|h^{V,V}|^2}{|h^{H,V}|^2} = XPD^H = \frac{|h^{H,H}|^2}{|h^{V,H}|^2} \quad (5.13)$$

The XPD measurement in [56] shows the symmetric leakage from V to H and H to V have the same power average, and if we ignore the small transmitted ray in media, see $E_{\text{Transmitted}}$ in Figure 5.4, we can assume $XPD^V = XPD^H$.

If we substitute $h^{x,y}$ ($x, y = V, H$) in equation (5.13), the XPD at the receiver can

be calculated as:

$$\begin{aligned} XPD^V &= \left(\frac{G_R^V}{G_R^H}\right)^2 \cot^2 \theta_r \\ XPD^H &= \left(\frac{G_R^H}{G_R^V}\right)^2 \cot^2 \theta_r \end{aligned} \quad (5.14)$$

As we see if rotation angle $\theta_r = 0$, the XPD reaches to infinity, but in a realistic environment the orientation of the receiver antenna is not aligned with the transmitter antenna, which results in a mismatch polarization. This means the XPD depends on both the receiver antenna's gain and the angle of incidence θ_r .

5.3.1 Full duplex PANC error probability analysis

The relay and the nodes are assumed to be synchronized and the channel state information is available at the receiver side for both transmit and broadcast channels. The channel coefficients h_{vv} and g_{vv} are mutually independent non-identical where

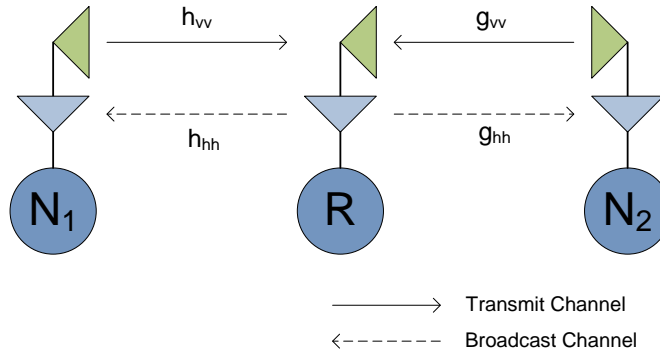


Figure 5.6: System model for a wireless TWRC full duplex PANC

$h_{vv} \sim \mathcal{CN}(m_h, \sigma_h^2)$ and $g_{vv} \sim \mathcal{CN}(m_g, \sigma_g^2)$. The means m_h and m_g are the complex Line-Of-Sight (LOS) components, where $k_h = \frac{|m_h|^2}{\sigma_h^2} \geq 0$, $k_g = \frac{|m_g|^2}{\sigma_g^2} \geq 0$ are the

Rice factors. Since the channel meets Rician fading, the PDF of the instantaneous SNR is a noncentral Chi-square distribution with PDF given [57, Eq.(5.10)]

$$P_{\gamma_{Ni}}(\gamma) = \frac{(K+1)}{\overline{\gamma_{Ni}}} e^{-\frac{K+(K+1)\gamma}{\overline{\gamma_{Ni}}}} I_0\left(2\sqrt{\frac{K(K+1)\gamma}{\overline{\gamma_{Ni}}}}\right) \quad i = 1, 2 \quad (5.15)$$

where K is Rician factor given by $K = \frac{\text{specular power}}{\text{random power}}$, and $\overline{\gamma_{Ni}} = \Omega_i P_{Ni}/N_o$ is the average SNR of node to relay, where P_{Ni}/N_o is the average transmit SNR at node and $\Omega_1 = \mathbb{E}\{h_{vv}^2\}$ or $\Omega_2 = \mathbb{E}\{g_{vv}^2\}$ are variances of h_{vv} or g_{vv} respectively, where $\mathbb{E}\{\cdot\}$ represents the statistical average operator. The transmit power P_{Ni} and variance N_o for the AWGN at the source nodes $N1, N2$ and the relay R is assumed to be equal.

$I_0(\cdot)$ is the zero-order modified Bessel function for the first kind. Note that $K > 0$ and $K = 0$ and $K = \infty$ respectively, corresponding to Rician and Rayleigh fading and AWGN non fading channel.

From Chapter 3.3.1 the end-to-end BER is written by

$$P_{N1 \rightarrow N2} = P_r^t + P_{r \rightarrow N2}^{t+1} - 2P_r^t P_{r \rightarrow N2}^{t+1} \quad (5.16)$$

where P_r^t is instantaneous BER at the relay for the transmit phase at time t , and $p_{r \rightarrow N2}^{t+1}$ is instantaneous BER during Broadcast phase from the relay to node-2 at time $t+1$.

The overall instantaneous end-to-end BER for given channel gains is written by

$$P_{inst} = \frac{1}{2}(P_{N1 \rightarrow N2} + P_{N2 \rightarrow N1}) \quad (5.17)$$

During the Broadcast phase the instantaneous BER from relay to node $P_{r \rightarrow Ni}$, $i = 1, 2$ in a Rician fading environment is given by Steins analysis [58]

$$P_{r \rightarrow Ni} = \frac{1}{2} [1 - Q_M(\sqrt{b}, \sqrt{a}) + Q_M(\sqrt{a}, \sqrt{b})] - \frac{A}{2} e^{(-\frac{a+b}{2})} I_0(\sqrt{ab}) \quad (5.18)$$

where [57, Eq.(8.150)]

$$\begin{aligned} \begin{Bmatrix} a \\ b \end{Bmatrix} &= \frac{1}{2} \left(\sqrt{\frac{\frac{K}{1+K} G \overline{\gamma_{Ni}}}{1 + \frac{1}{1+K} G \overline{\gamma_{Ni}}}} \mp \sqrt{\frac{\frac{K}{1+K} \overline{\gamma_{Ni}}}{1 + \frac{1}{1+K} \overline{\gamma_{Ni}}}} \right)^2 \\ A &= \frac{\frac{\sqrt{G}}{1+K} \overline{\gamma_{Ni}}}{\sqrt{\left(\frac{G}{1+K} \overline{\gamma_{Ni}} + 1 \right) \left(\frac{1}{1+K} \overline{\gamma_{Ni}} + 1 \right)}} \end{aligned} \quad (5.19)$$

G is the SNR gain of the reference signa $G = SNR_{ref}/(E_b/N_o)$ [59] and $Q_M(.,.)$ is the first-order Marcum Q function and I_0 is the zero-order modified Bessel function of the first kind.

As mentioned before for Rayleigh fading channel $K = 0$ would result in

$$\begin{Bmatrix} a \\ b \end{Bmatrix} = \begin{Bmatrix} 0 \\ 0 \end{Bmatrix}, \quad A = \frac{\sqrt{G \overline{\gamma_{Ni}}}}{\sqrt{(G \overline{\gamma_{Ni}} + 1)(\overline{\gamma_{Ni}} + 1)}} \quad (5.20)$$

where $Q_M(0, 0) = 1$ and according 5.18 obtains

$$P_{r \rightarrow Ni} = \frac{1}{2} \left(1 - \frac{\sqrt{G \overline{\gamma_{Ni}}}}{\sqrt{(G \overline{\gamma_{Ni}} + 1)(\overline{\gamma_{Ni}} + 1)}} \right) \quad (5.21)$$

For a perfect phase reference $G \rightarrow \infty$ we get

$$P_{r \rightarrow Ni} = \frac{1}{2} \left(1 - \sqrt{\frac{\overline{\gamma_{Ni}}}{1 + \overline{\gamma_{Ni}}}} \right) \quad (5.22)$$

which is consistent with the result given in Proakis [42]. For AWGN channel $K \rightarrow \infty$ and $\overline{\gamma_{Ni}} \rightarrow E_b/N_o$ result are

$$\left\{ \begin{array}{l} a \\ b \end{array} \right\} = \frac{1}{2} \left(\sqrt{G \frac{E_b}{N_o}} \mp \sqrt{\frac{E_b}{N_o}} \right)^2 = \frac{E_b}{2N_o} (\sqrt{G} \mp 1)^2, \quad A = 0 \quad (5.23)$$

Outage probability : The instantaneous end-to-end SNR at nodes during the Broadcast phase can be given by [60]

$$\gamma_{N1 \rightarrow N2} = \gamma_r = \frac{\gamma_{N1} \gamma_{N2}}{\gamma_{N1} + \gamma_{N2}} \quad (5.24)$$

End-to-end outage probability is defined as the probability that the instantaneous end-to-end SNR falls below a threshold γ_{th} .

$$P_{out} = F_{\gamma_r}(\gamma_{th}) = P_r [\gamma_r < \gamma_{th}] \quad (5.25)$$

To calculate end-to-end outage probability at one of the source nodes, it is shown in [60, Eq.(29)] that $p_{\gamma_r}(\gamma)$ can be expressed as

$$p_{\gamma_r}(\gamma) = \int_{\gamma}^{\infty} \frac{x^2}{(x - \gamma)^2} p_{\gamma_h} \left(\frac{\gamma x}{x - \gamma} \right) p_{\gamma_g}(x) dx \quad (5.26)$$

where p_{γ_h} and p_{γ_g} are PDF of γ_h and γ_g for the respective channel. By applying

PDF of Rician distribution 5.15 in 5.26 we get

$$\begin{aligned}
p_{\gamma_r}(\gamma) &= \int_{\gamma}^{\infty} \frac{x^2}{(x-\gamma)^2} \frac{(K_h+1)}{\bar{\gamma}_h} e^{\left(-K_h - \frac{(K_h+1)\gamma x}{\bar{\gamma}_h(x-\gamma)}\right)} \\
&\times I_0 \left(2\sqrt{\frac{K_h(K_h+1)\gamma x}{\bar{\gamma}_h(x-\gamma)}} \right) \\
&\times \frac{(K_g+1)}{\bar{\gamma}_g} e^{\left(-K_g - \frac{(K_g+1)x}{\bar{\gamma}_g}\right)} I_0 \left(2\sqrt{\frac{K_h(K_h+1)x}{\bar{\gamma}_g}} \right) dx. \quad (5.27)
\end{aligned}$$

After simplifying by using the identities [61, Eq.(8.447.1)], we get

$$\begin{aligned}
p_{\gamma_r}(\gamma) &= \int_0^{\infty} \frac{(x+\gamma)^2}{x^2} \frac{(K_h+1)}{\bar{\gamma}_h} e^{\left(-K_h - \frac{(K_h+1)\gamma(x+\gamma)}{\bar{\gamma}_h x}\right)} \\
&\times \sum_{m=0}^{\infty} \frac{1}{(m!)^2} \left(\frac{K_h(K_h+1)\gamma(x+\gamma)}{\bar{\gamma}_h x} \right)^m \\
&\times \frac{(K_g+1)}{\bar{\gamma}_g} e^{\left(-K_g - \frac{(K_g+1)(x+\gamma)}{\bar{\gamma}_g}\right)} \\
&\times \sum_{n=0}^{\infty} \frac{1}{(n!)^2} \left(\frac{K_h(K_h+1)(x+\gamma)}{\bar{\gamma}_g} \right)^n dx. \quad (5.28)
\end{aligned}$$

Rearranging terms, we get

$$\begin{aligned}
p_{\gamma_r}(\gamma) &= \frac{(K_h+1)(K_g+1)}{\bar{\gamma}_h \bar{\gamma}_g} e^{\left(-K_h - K_g - \frac{(K_h+1)\gamma}{\bar{\gamma}_h} - \frac{(K_g+1)\gamma}{\bar{\gamma}_g}\right)} \\
&\times \sum_{m=0}^{\infty} \sum_{n=0}^{\infty} \frac{1}{(n!(m-n)!)^2} \left(\frac{K_h(K_h+1)\gamma}{\bar{\gamma}_h} \right)^n \left(\frac{K_h(K_h+1)}{\bar{\gamma}_g} \right)^{m-n} \\
&\times \int_0^{\infty} x^{m-n} (1+\gamma x^{-1})^{m+2} e^{\left(-\frac{(K_h+1)\gamma^2}{\bar{\gamma}_h x} - \frac{(K_g+1)x}{\bar{\gamma}_g}\right)} dx. \quad (5.29)
\end{aligned}$$

By expanding the term $(1 + \gamma x^{-1})^{m+2}$ with the help of [61, Eq.(1.111)] yield

$$\begin{aligned}
p_{\gamma_r}(\gamma) &= \frac{(K_h + 1)(K_g + 1)}{\bar{\gamma}_h \bar{\gamma}_g} e^{\left(-K_h - K_g - \frac{(K_h + 1)\gamma}{\bar{\gamma}_h} - \frac{(K_g + 1)\gamma}{\bar{\gamma}_g}\right)} \\
&\times \sum_{m=0}^{\infty} \sum_{n=0}^{\infty} \frac{1}{(n!(m-n)!)^2} \left(\frac{K_h(K_h + 1)\gamma}{\bar{\gamma}_h}\right)^n \left(\frac{K_h(K_h + 1)}{\bar{\gamma}_g}\right)^{m-n} \\
&\times \sum_{k=0}^{m+2} \binom{m+2}{k} \gamma^k \int_0^{\infty} x^{m-n-k} e^{\left(-\frac{(K_h + 1)\gamma^2}{\bar{\gamma}_h x} - \frac{(K_g + 1)x}{\bar{\gamma}_g}\right)} dx. \tag{5.30}
\end{aligned}$$

Following [61, Eq.(3.471.9)] yielding the compact PDF of γ_r expresses

$$\begin{aligned}
p_{\gamma_r}(\gamma) &= \frac{(K_h + 1)(K_g + 1)}{\bar{\gamma}_h \bar{\gamma}_g} e^{\left(-K_h - K_g - \frac{(K_h + 1)\gamma}{\bar{\gamma}_h} - \frac{(K_g + 1)\gamma}{\bar{\gamma}_g}\right)} \\
&\times \sum_{m=0}^{\infty} \sum_{n=0}^{\infty} \frac{1}{(n!(m-n)!)^2} \left(\frac{K_h(K_h + 1)}{\bar{\gamma}_h}\right)^n \left(\frac{K_h(K_h + 1)}{\bar{\gamma}_g}\right)^{m-n} \\
&\times \sum_{k=0}^{m+2} \binom{m+2}{k} 2\gamma^{m+1} \left(\sqrt{\frac{(K_h + 1)\gamma_g}{(K_g + 1)\gamma_h}}\right)^{(m-n-k+1)} \\
&\times I_{m-n-k+1} \left(2\gamma \sqrt{\frac{(K_h + 1)(K_g + 1)}{\gamma_h \gamma_g}}\right). \tag{5.31}
\end{aligned}$$

where $I_v(\cdot)$ is v th-order modified Bessel function of the second kind defined in [61, Eq.(8.432.6)], and K_h and K_g are the Rician K factor the h and g channel respectively.

For Rayleigh fading channel where $K_h = 0$ and $K_g = 0$ we get

$$\begin{aligned}
p_{\gamma_r}(\gamma) &= \frac{2\gamma}{\bar{\gamma}_h \bar{\gamma}_g} e^{\left(-\frac{\gamma}{\bar{\gamma}_h} - \frac{\gamma}{\bar{\gamma}_g}\right)} \left(\sqrt{\frac{\bar{\gamma}_g}{\bar{\gamma}_h}} + \sqrt{\frac{\bar{\gamma}_h}{\bar{\gamma}_g}}\right) \\
&\times I_1 \left(\frac{2\gamma}{\sqrt{\bar{\gamma}_h \bar{\gamma}_g}}\right) + 2I_0 \left(\frac{2\gamma}{\sqrt{\bar{\gamma}_h \bar{\gamma}_g}}\right). \tag{5.32}
\end{aligned}$$

which is in agreement with the result from [62].

The general formula for average bit error probability as given in [63] $P_b(e|\gamma) = aE_\gamma(Q(\sqrt{2b\gamma}))$, where $Q(x) = \frac{1}{\sqrt{2\pi}} \int_x^\infty e^{-\frac{y^2}{2}} dy$, and for BPSK $a=1$ and $b=1$, and for QPSK $a=1$ and $b=0.5$, where for our case (BPSK) leads to

$$P_b = \frac{1}{2\sqrt{\pi}} \int_0^\infty \frac{P_{\gamma_r}(t)}{\sqrt{t}} e^{-t} dt \quad (5.33)$$

Substituting 5.31 in above equation, we get

$$\begin{aligned} P_b &= \frac{1}{2\sqrt{\pi}} \int_0^\infty \frac{1}{\sqrt{\gamma}} e^{-\gamma \frac{(K_h+1)(K_g+1)}{\bar{\gamma}_h \bar{\gamma}_g}} e^{\left(-K_h - K_g - \frac{(K_h+1)\gamma}{\bar{\gamma}_h} - \frac{(K_g+1)\gamma}{\bar{\gamma}_g}\right)} \\ &\times \sum_{m=0}^\infty \sum_{n=0}^\infty \frac{1}{(n!(m-n)!)^2} \left(\frac{K_h(K_h+1)}{\bar{\gamma}_h}\right)^n \left(\frac{K_h(K_h+1)}{\bar{\gamma}_g}\right)^{m-n} \\ &\times \sum_{k=0}^{m+2} \binom{m+2}{k} 2\gamma^{m+1} \left(\sqrt{\frac{(K_h+1)\gamma_g}{(K_g+1)\gamma_h}}\right)^{(m-n-k+1)} \\ &\times I_{m-n-k+1} \left(2\gamma \sqrt{\frac{(K_h+1)(K_g+1)}{\gamma_h \gamma_g}}\right) d\gamma. \end{aligned} \quad (5.34)$$

By using identities [61, Equations 3.361.2 and 6.621.3] the end to end BER can be

expressed as

$$\begin{aligned}
P_b &= \frac{1}{2\sqrt{\pi}} \frac{(K_h + 1)(K_g + 1)}{\bar{\gamma}_h \bar{\gamma}_g} e^{(-K_h - K_g)} \sum_{m=0}^{\infty} \sum_{n=0}^{\infty} \frac{1}{(n!(m-n)!)^2} \\
&\times \left(\frac{K_h(K_h + 1)}{\bar{\gamma}_h} \right)^n \left(\frac{K_h(K_h + 1)}{\bar{\gamma}_g} \right)^{m-n} \\
&\times \sum_{k=0}^{m+2} \binom{m+2}{k} 2 \left(\sqrt{\frac{(K_h + 1)\gamma_g}{(K_g + 1)\gamma_h}} \right)^{(m-n-k+1)} \\
&\times \frac{\pi \left(4\sqrt{\frac{(K_h + 1)(K_g + 1)}{\gamma_h \gamma_g}} \right)^{m-n-k+1}}{\left(-\frac{(K_h + 1)}{\bar{\gamma}_h} - \frac{(K_g + 1)}{\bar{\gamma}_g} + 2\sqrt{\frac{(K_h + 1)(K_g + 1)}{\gamma_h \gamma_g}} \right)^{2m-n-k+3}} \\
&\times \frac{\Gamma(2m - n - k + 3)\Gamma(n + k + 1)}{\Gamma(m + \frac{3}{2})} \\
&\times F \left(2m - n - k + 3, m - n - k + \frac{3}{2}; m + \frac{3}{2}; \right. \\
&\quad \left. \frac{\left(-\frac{(K_h + 1)}{\bar{\gamma}_h} - \frac{(K_g + 1)}{\bar{\gamma}_g} - 2\sqrt{\frac{(K_h + 1)(K_g + 1)}{\gamma_h \gamma_g}} \right)}{\left(-\frac{(K_h + 1)}{\bar{\gamma}_h} - \frac{(K_g + 1)}{\bar{\gamma}_g} + 2\sqrt{\frac{(K_h + 1)(K_g + 1)}{\gamma_h \gamma_g}} \right)} \right) \tag{5.35}
\end{aligned}$$

where $F(.,.,.;.)$ is the hypergeometric function defined in [61, Equations 9.111] and $\Gamma(.)$ is the Gamma function defined in [61, Equations 8.310.1]. This close form gives an end-to-end average BER over two way relay symmetric Rician fading channels.

5.3.2 Simulations and results

During the transmit phase, the two nodes simultaneously transmit BPSK signals to the relay. The receive signal at the relay is given by:

$$r = h_{vv}x_1 + g_{vv}x_2 + n \tag{5.36}$$

where x_i is the transmitted signal $x_i \in \{1, -1\}$ and h_{vv} and g_{vv} are channel coefficients $h_i \sim \mathcal{CN}(0, \sigma^2)$ with zero mean and variance σ^2 , and n is the additive white gaussian noise.

The channel matrix for a cross-polarization (CP) antenna is presented by equation (5.8) and (5.8) but for our system full duplex PANC, according to the Figure 5.7 the general LOS/NLOS channel matrix is

$$H_{CP} = \begin{bmatrix} H_{n \times m}^{VV} & H_{n \times m}^{VH} \cdot A_z \\ H_{n \times m}^{HV} & H_{n \times m}^{HH} \cdot A_z \end{bmatrix} \quad H_{FD} = \begin{bmatrix} H_{n \times m}^{VV} & H_{n \times m}^{HV} \cdot A_z \\ H_{n \times m}^{VH} & H_{n \times m}^{HH} \cdot A_z \end{bmatrix} \quad (5.37)$$

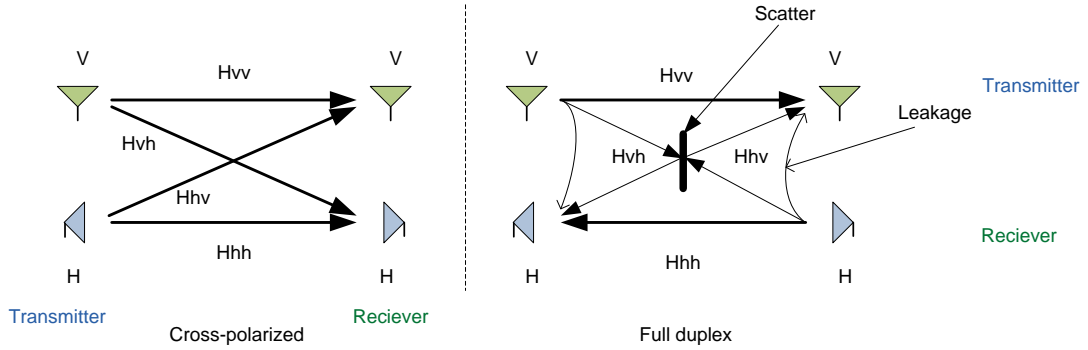


Figure 5.7: Cross-polarized system vs. full duplex system

For channel simulation two Gaussian random variables L and N considered, where L has modeled as specular component (LOS) and N as scatter component. The L has non-central Chi Square distribution due to non-zero mean m while the N has central Chi Square distribution due to zero mean and both have equal variance σ^2 . The transformation $r = \sqrt{L^2 + N^2}$ yield Rician distribution. Therefore k -factor, as defined in the previous section is given by $k = \frac{m}{2\sigma^2}$. According to this equation the

mean m and the average power σ defines as

$$\begin{aligned} m &= \sqrt{\frac{k}{k+1}} \\ \sigma &= \sqrt{\frac{1}{2(k+1)}} \end{aligned} \quad (5.38)$$

For simulation, the distance between the relay and each node is chosen to be $D=100\text{m}$, with a carrier frequency of $f=5\text{ GHz}$. To be more realistic, the azimuthal displacement angle of the relay and nodes antennas have been taken into account, and assumed to be 30° , which is added for all the horizontally polarized transmitting signals. The polarization rotation angle in a cross-polarized antenna θ_p for V-H and H-V components, and polarization rotation angle between nodes and relay antenna θ_a for V-V and H-H components has been chosen as $\theta_p = \theta_a = 5^\circ$ which is very small. At the relay maximum likelihood (ML) detection is employed.

The error probability is displayed in Figure 5.8 for k-factor 0 dB and 10 dB. It can be seen that the bit error probability rate closely matches the actual bit error probability rate. It is also shown that when the k-factor increases the bit error probability of the system will decrease.

The result was compared with single antenna two way relay networking, which shows that the error probability closely matches the polarized relay error probability when k factor is 0 dB.

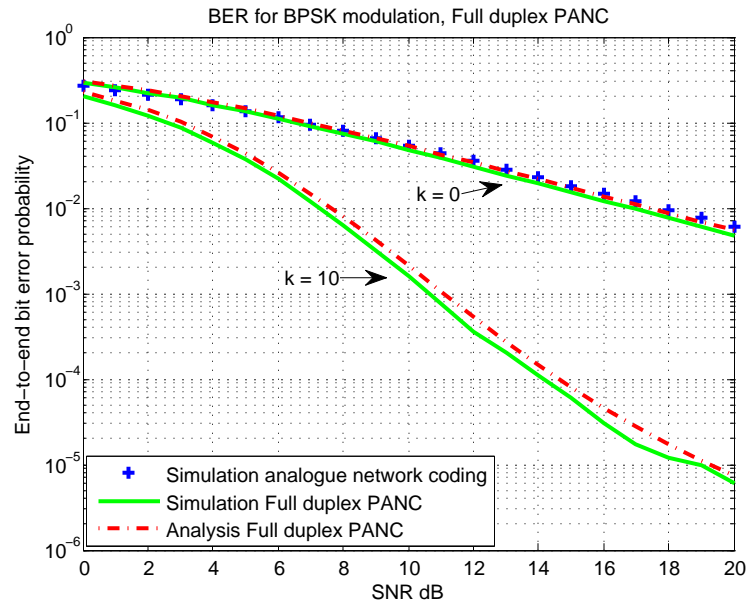


Figure 5.8: Bit error probability as a function of SNR for different K-factor for SNR = 10 dB

In the next simulation I investigated the influence of k-factor on the full duplex PANC system. The channel parameters were same as previous simulations, except fixed SNR value for 10 dB. It is clear from Figure 5.9 that system performance improves with increasing k-factor. This is with no doubt shown that at high k-factor, the system behaves like an AWGN link and outperforms a fading channel with the same average channel power.

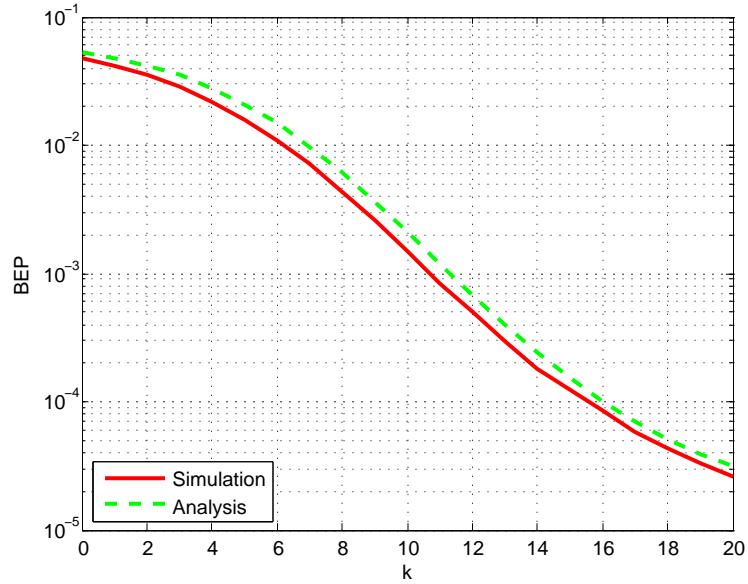


Figure 5.9: Bit error probability as a function of K-factor

Figure 5.10 shows the effect of polarization rotation angle LOS and propagation environment NLOS (coupling between orthogonal polarizations due to scattering) θ_a from 0° to 90° on system performance. It is obvious when the transmitter and receiver antennas polarization rotation angle increases from strictly aligned antennas, namely co-polarized antennas $\theta_a = 0^\circ$, to orthogonally oriented antennas $\theta_a = 90^\circ$ the performance of the system decreases. Figure 5.10 also shows the effect of the cross-polarized rotation angle θ_p between elements inside the antennas (antennas' elements mismatched) or leakage for $\theta_p = 0^\circ, 5^\circ, 20^\circ$. The effect of the cross-polarized rotation angle below 5° is almost negligible, which in a realistic fabrication of an antenna, can not be more than $\theta_p = 5^\circ$. As we see for $\theta_p = 20^\circ$ the system performance does drop-off.

The XPD for our relay system according to equation (5.13) can be written as

$$XPD^V = \frac{|h^{V,V}|^2 + |g^{V,V}|^2}{|h^{H,V}|^2} = XPD^H = \frac{|h^{H,H}|^2 + |g^{H,H}|^2}{|h^{V,H}|^2} \quad (5.39)$$

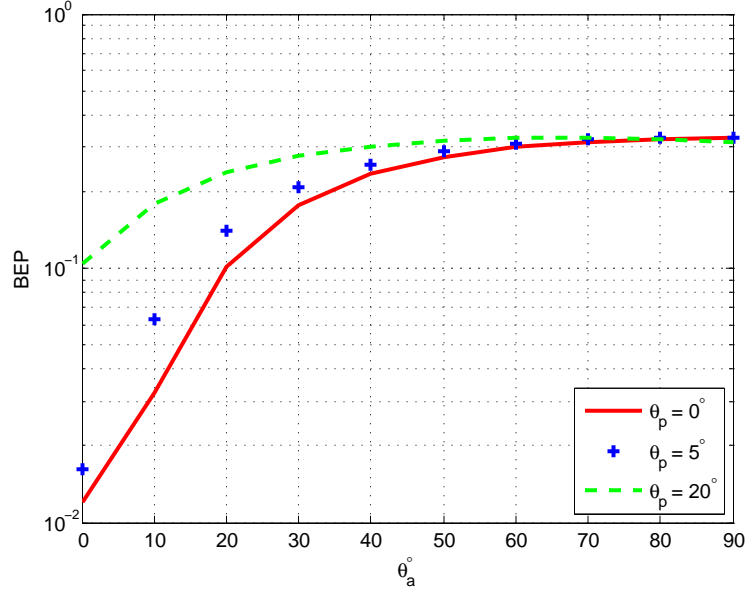


Figure 5.10: Polarization rotation angle

Because $g^{H,V} = h^{H,V}$ and $h^{V,H} = g^{V,H}$ we can rewrite the above equation as well as

$$XPD^V = \frac{|h^{V,V}|^2 + |g^{V,V}|^2}{|g^{H,V}|^2} = XPD^H = \frac{|h^{H,H}|^2 + |g^{H,H}|^2}{|g^{V,H}|^2} \quad (5.40)$$

Figure 5.11 and 5.12 portray the XPD for different Rx/Tx rotation angles at the relay when SNR 10 dB, $k = 10$, distance $D=100$ m and azimuthal displacement angle is assumed to be 30° . From this figure we can observe that, the XPD_V transmitter channel is usually larger than the XPD_H broadcast channel, because of the azimuthal rotation angle. Notice the difference between the azimuthal effect and the reflection effect on the vertically polarized signal. In reality, reflection of vertically polarized waves is less efficient, so vertical polarization is less susceptible to multipath fading due to ground-based reflection, whose measurements show that the XPD_V transmitter is larger than XPD_H [64], because the vertically polarized

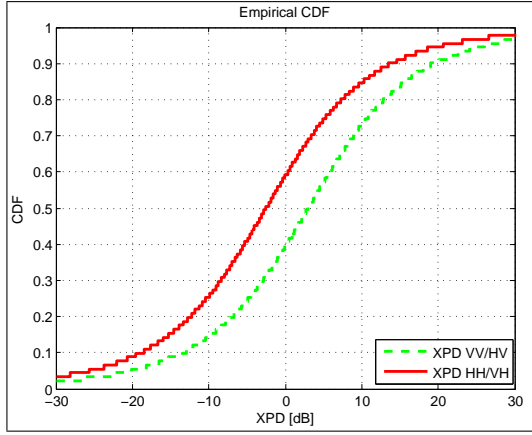


Figure 5.11: CDF function of XPD

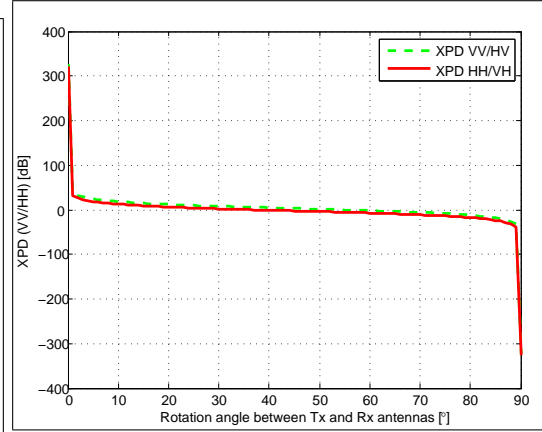


Figure 5.12: XPD function of antenna rotation angle

signal is preferable during the propagation.

As we see in the Figures, the XPD strongly depends on the polarization rotation angle between the antennas, and shows the potential of a mismatch between the Tx/Rx antenna's polarization angle to increase co-channel (transmitter/broadcast channel) interference and decrease channel capacity. In an ideal situation where transmitter and receiver antenna elements are strictly orthogonal, i.e. rotation angle is 0° , XPD is infinity, and as the rotation angle increases XPD decreases to 0° . Note that in Figure 5.12 when the rotation angle is about 45° the XPD_H is 1, while the XPD_V for 60° is 1. The reason is the effect of azimuthal on H-H link which make the XPD_V higher than the XPD_H .

5.4 TWRC polarization diversity

One of the effective ways to improve performance of a wireless system is diversity. In this section cross-polarized antenna TWRC diversity was studied and compared with MIMO 2x2 antenna TWRC diversity, and with the proposed system from the previous section and also with the single antenna TWRC from Chapter 3.3 which

deals with whiteout impulsive noise.

Theoretical performance analysis and measurement of cross-polarized antennas was evaluated and studied [65], [66]. In general it is possible to consider transmission between two dual polarized antennas e.g. cross-polarized antennas in a similar way as if there were 2 transmit and 2 receive antennas, resulting in 4 sub-channels, each characterized by its own complex channel gain much the same as in the case of a 2x2 MIMO system.

If we assume that signal x transmits by horizontal and vertical antennas of node-1 and y transmits by horizontal and vertical antennnas of node-2, the received signal at relay r_1 and r_2 are:

$$\begin{aligned} r_1 &= (x \cdot h_{hh} + x \cdot h_{vh}) \oplus (y \cdot g_{hh} + y \cdot g_{vh}) \\ r_2 &= (x \cdot h_{vh} + x \cdot h_{vv}) \oplus (y \cdot g_{vh} + y \cdot g_{vv}) \end{aligned} \quad (5.41)$$

where χ_{hh} , χ_{vh} , χ_{hv} and χ_{vv} , $\chi = \{h, g\}$ are channel coefficients for transmission between node and relay horizontal and horizontal, vertical and horizontal, horizontal and vertical, and vertical and vertical antennas respectively. Finally the receive antenna relay system is: $r = r_1 + r_2$.

For simulation I assumed the distance between the relay and each node is $D=100\text{m}$. The carrier frequency $f=5\text{ GHz}$, polarization rotation angle between transmitter and receiver antennas and azimuthal displacement angle is 30° . And for a fair comparison Rician k-factor was chosen 0 dB, for no Rician fading channel (pure Rayleigh fading). At the relay maximum likelihood (ML) detection was employed.

It is also assumed that the total transmit power is the same for all scenarios and the receiver has perfect knowledge of the channel. The results provide a good reference performance for designers.

As shown in Figure 5.13 the performance of the cross-polarized antenna relay diversity is 8 dB better than the MIMO antenna relay diversity, which in its turn has better performance compared to those two other systems.

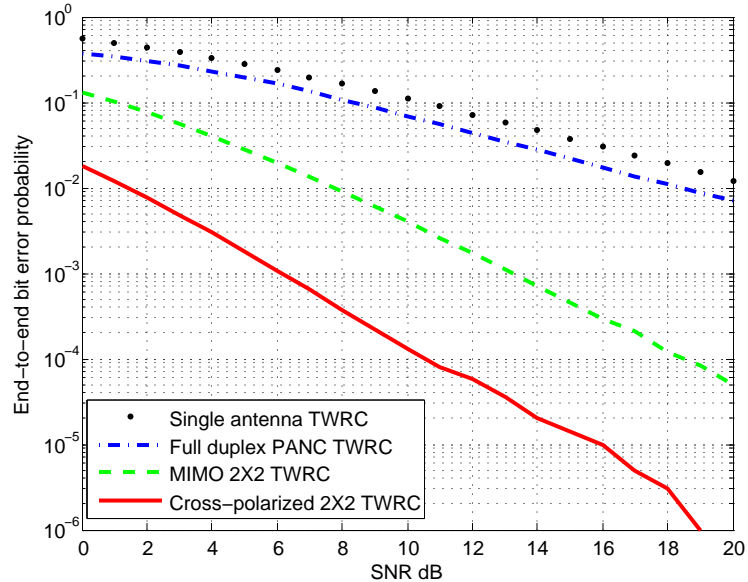


Figure 5.13: Comparison of MIMO cross-polarized antenna TWRC with MIMO TWRC scenarios, $k=0$

This result shows that the cross-polarized antenna TWRC system provides more robust and efficient transmission compared to the other TWRC transmission systems, particularly when there is a very low polarization mismatch for the cross-polarized antenna TWRC system, because the antennas are always fixed and the rotation angle between the receiver and transmitter antenna is small, except for movement of scatters around the system. The other advantage of the cross-polarized antenna TWRC system is that it is a cost- and space- effective alternative, where two spatially separated uni-polarized antennas are replaced by a single antenna with orthogonal polarization.

The last simulation investigates two cross-polarized or MIMO polarized antenna

TWRC systems and the results were compared with the single cross-polarized antenna TWRC system. The MIMO Polarized diversity is an effective solution to increase system performance, but a separation of several wavelengths between antennas is usually needed in order to keep mutual correlation between cross-polarized antennas at an acceptable level to achieve significant diversity gain. The MIMO polarized antenna is a promising cost- and space-effective alternative. For the MIMO polarized antenna TWRC system we can use the same principal as equation (5.41), just extend it to the dual cross-polarized antenna TWRC system. Each of the channel matrixes for the MIMO polarized antenna TWRC system are expressed as 4x4 dimensions. Obviously simulation results show an increase in performance of the TWRC system when the MIMO polarized antenna is applied.

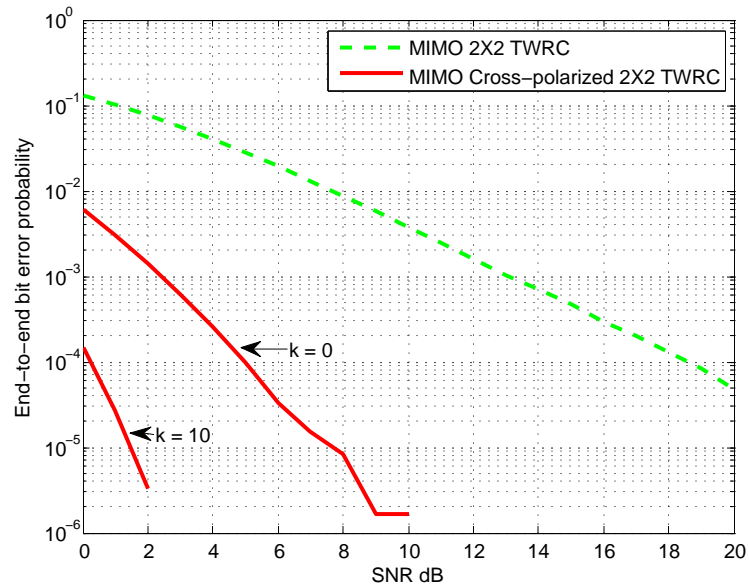


Figure 5.14: Comparison of cross-polarized TWRC with MIMO 2X2 TWRC, $k=0$

5.5 Polarized Multicast Two Way Relay Channel (PM-TWRC)

To meet future demands we need to have multicast² systems. For instance high priority data must deliver in less than a few milliseconds. Addressing this challenge requires not only a communication system without delays, but also avoidance of buffering packets in node(s)/relay(s). To this end, by giving higher priority to control data in the buffer queue, to some extent it is possible to solve this issue but it is not an efficient way.

Instead, I propose a dual multicast communication system based on channel polarized systems, which was explained in the previous Chapter.

To this end, as Figure 5.15 shows, a node/relay simultaneously can handle both high and low priority signals by assigning a polarized antenna to a particular transmission path. In other words, the high priority signals have their own path and own buffer system. The advantages to having a distinct transmission channel for polarized antennas are that node(s)/relay(s) do not need to have a different carrier frequency for each transmission or the transmission channel do not need to use separate node(s)/relay(s) for different transmission priorities. The other advantages is that node(s)/relay(s) can adaptively alter channels between the higher or lower priority signals depending on demands. I named this transmission system “Polarized

2. **Unicast or point to point** describe communication where information is sent from one point to another point. In this case there is just one sender, and one receiver.

Broadcast describe communication where information is sent from one point to all other points. In this case there is just one sender, but the information is sent to all connected receivers.

Multicast describe communication information is sent from one or more points to a set of other points. In this case there is may be one or more senders, and the information is distributed to a set of receivers.

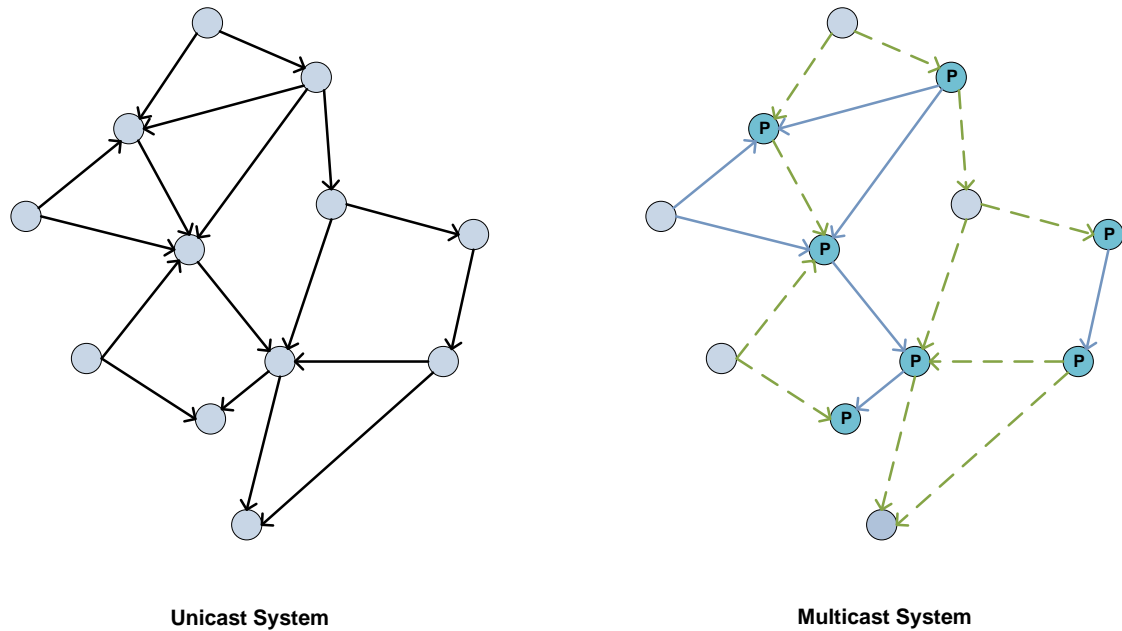


Figure 5.15: Unicast system vs. multicast system

Multicast Two Way Relay Channel” or “PM-TWRC”.

As shown in Figure 5.15 node(s)/relay(s) marked with the letter “p” and linked with the dashed line are dual polarized while other node(s)/relay(s) and links may be dual- or uni-polarized. A simple example can be when a user send smart meter data thorough the same transmission links and node(s)/relay(s) as SCADA data is being sent.

5.5.1 Polarized Multi Path TWRC (PMP-TWRC)

The other use of the Polarized Multicast TWRC system is that it allows application data to use multiple paths to maximize resource usage and increase redundancy. This can be implemented in the relay(s) by a simple algorithm. This means the effect from the loss of a polarized antenna transmission can be negated by rerouting signals through alternate polarized antenna. I named this transmission system

Polarized Multi Path TWRC (PM-TWRC) system.

5.6 Conclusions

By means of polarization we are able to achieve spectral efficiency via spatial multiplexing, and improve the reliability by spatial diversity. Indeed, multiple dual polarized (DP) and single polarized (SP) antennas are appealing for use in 4G LTE systems. I proposed a new TWRC scheme based on polarization, which is able to transmit and receive data between nodes simultaneously by using the same carrier frequency. The proposed system improves spectral efficiency, data rate, capacity and link reliability.

I imposed and analyzed polarization diversity on the TWRC system and compared it with a single antenna TWRC system and a MIMO TWRC system in a fading channel. It is shown that the polarization diversity has better performance than a non-polarized antenna TWRC system.

Finally I proposed a new architecture for a multicast TWRC system for improvement of the system delay, namely PM-TWRC system.

Chapter 6

Conclusions and future work

The purpose of this thesis was to investigate the performance of a Two Way Relay Channel (TWRC) systems and determine the gaps in existing research.

It is known that impulsive noise can deteriorate the overall system performance drastically in a communication system. Therefore TWRC system performance was evaluated in such an environment. Simulations were done for different scenarios by varying impulsive noise intensity. To mitigate the effect of impulsive noise in such environments, Viterbi decoding algorithm was implemented and simulated.

A dynamic modulation increase reliability of transmission, therefore Adaptive Coding and Modulation (ACM) was considered for the TWRC system. Hence simulation was done for a TWRC Asymmetric Modulation (AM) system.

Because there are extra transmission in an asymmetric TWRC system, I have proposed and simulated a new algorithm which I call an Optimal Decision Decoding Algorithm (ODDA). In this part I also did a study on the effect of various signal constellations in a asymmetric TWRC.

Spatial diversity dramatically increases performance and range of a wireless system, thus I did a study of a multi antenna TWRC system. I did simulations both for a MISO Alamouti scheme and a MIMO system in an impulsive noise environment and compared them to a single antenna TWRC system.

Future work should include the study of efficient algorithms for the transport layer. There also should be a study of a hybrid architecture for future demands, that includes a variety of communication techniques.

In the second part, I proposed a new full duplex TWRC scheme based on polarization, which I call full duplex Polarized Antenna Network Coding (full duplex PANC) system. The aim behind this work was to achieve a lower delay in TWRC systems for high priority data communication system, which is a critical issue, while using the same channel resources or carrier frequency.

There are multiple challenges related to this work, therefore the model was analysed for Rician and Rayleigh fading channel and Rician k-factor and antennas rotation angles. I did simulations for the proposed system, by considering the antenna rotation angle between the transmitter and receiver including the angle between the dual polarized antenna for the transmitter and receiver.

The cross-polarized and MIMO polarized TWRC system was investigated too, and compared with other systems. Obviously the MIMO polarized TWRC has the best performance with the cost of an extra polarized antenna, but the cross-polarized system has advantages in that it does not need an extra antenna, and both polarized elements can be implemented in one antenna.

Finally I have proposed a new topology for a TWRC system which is based on a dual polarization antenna. Thus I call it a Polarized Multicast Two Way Relay Channel (PM-TWRC) system. The PM-TWRC system uses dual multicast networks, which are able to dedicate one of the dual multicast networks to high priority data or can make use of both multicast networks simultaneously, which I named as Polarized Multi Path TWRC (PMP-TWRC). The PMP-TWRC system is a redundant network to increase the reliability of the system.

Future work involves investigation for leakage between the two adjacent polarized

antennas, which directly depends on the distance between the polarized antennas. It may be necessary to investigate for leakage between two polarized elements in an antenna.

Bibliography

- [1] G. Bedicks, C. Dantas, F. Sukys, F. Yamada, L. Raunheite, and C. Akamine, “Digital signal disturbed by impulsive noise,” *Broadcasting, IEEE Transactions on*, vol. 51, no. 3, pp. 322 – 328, sept. 2005. 2
- [2] R. Shepherd, “Measurements of amplitude probability distributions and power of automobile ignition noise at hf,” *Vehicular Technology, IEEE Transactions on*, vol. 23, no. 3, pp. 72 – 83, aug 1974. 2
- [3] A. Spaulding and D. Middleton, “Optimum reception in an impulsive interference environment—part i: Coherent detection,” *Communications, IEEE Transactions on*, vol. 25, no. 9, pp. 910 – 923, sep 1977. 2, 29
- [4] D. Middleton, “Non-gaussian noise models in signal processing for telecommunications: new methods and results for class a and class b noise models,” *Information Theory, IEEE Transactions on*, vol. 45, no. 4, pp. 1129 –1149, may 1999. 2
- [5] K. J. Ray Liu, A. K. Sadek, W. Su, and A. Kwasinski, *Cooperative Communications and Networking*. Cambridge, UK: Cambridge University, 2008. 2
- [6] S. Zhang, S. chang Liew, and P. P. Lam, “Physical-layer network coding,” in *ACM Mobicom '06*, 2006, pp. 358–365. 2

-
- [7] R. Pickholtz, D. Schilling, and L. Milstein, “Theory of spread-spectrum communications—a tutorial,” *Communications, IEEE Transactions on*, vol. 30, no. 5, pp. 855 – 884, may 1982. 4
- [8] R. A. S. M. K. Simon, J. K. Omura and B. K. Levitt., *Spread Spectrum Communications Handbook*. New York, NY, USA: McGraw-Hill Companies, 1994. 4
- [9] A. Viterbi, “Spread spectrum communications—myths and realities,” *Communications Magazine, IEEE*, vol. 17, no. 3, pp. 11 – 18, may 1979. 4
- [10] D. Torrieri, “Mobile frequency-hopping cdma systems,” *Communications, IEEE Transactions on*, vol. 48, no. 8, pp. 1318–1327, 2000. 4
- [11] V. Gungor, B. Lu, and G. Hancke, “Opportunities and challenges of wireless sensor networks in smart grid,” *Industrial Electronics, IEEE Transactions on*, vol. 57, no. 10, pp. 3557 –3564, oct. 2010. 7, 9, 10
- [12] E. N. Skomal, *Man-Made Radio Noise*. New York, NY, USA: Van Nostrand Reinhold, 1978. 7, 9
- [13] J. D. Parsons and J. G. Gardiner, *Mobile Communication Systems*. New York, NY, USA: Halsted Press, 1989. 8, 9
- [14] A. Bodonyi, “Effects of impulse noise on digital data transmission,” *Communications Systems, IRE Transactions on*, vol. 9, no. 4, pp. 355 –361, december 1961. 8
- [15] K. Blackard, T. Rappaport, and C. Bostian, “Radio frequency noise measurements and models for indoor wireless communications at 918 mhz, 2.44 ghz,

- and 4.0 ghz,” in *Communications, 1991. ICC '91, Conference Record. IEEE International Conference on*, jun 1991, pp. 28 –32 vol.1. 8
- [16] G. Maxam, H. Hsu, and P. Wood, “Radiated ignition noise due to the individual cylinders of an automobile engine,” *Vehicular Technology, IEEE Transactions on*, vol. 25, no. 2, pp. 33 – 38, may 1976. 9
- [17] J. Cheah, “Interference characteristics of microwave ovens in indoor radio communications,” in *Personal, Indoor and Mobile Radio Communications., IEEE International Symposium on*, sep 1991, pp. 280 –285. 9, 10
- [18] K. Blackard, T. Rappaport, and C. Bostian, “Measurements and models of radio frequency impulsive noise for indoor wireless communications,” *Selected Areas in Communications, IEEE Journal on*, vol. 11, no. 7, pp. 991 –1001, sep 1993. 9
- [19] O. Batur, M. Koca, and G. Dunder, “Measurements of impulsive noise in broad-band wireless communication channels,” in *Research in Microelectronics and Electronics, 2008. PRIME 2008. Ph.D.*, 22 2008–april 25 2008, pp. 233 –236. 9
- [20] A. Shukla, “Feasibility study into the measurement of man-made noise,” *Defence Evaluation Research Agency (DERA): Radiocommunications Agency: UK. Ministry of Defence*, pp. 1 – 65, Mar 2001. 9
- [21] T. Blankenship and T. Rappaport, “Characteristics of impulsive noise in the 450-mhz band in hospitals and clinics,” *Antennas and Propagation, IEEE Transactions on*, vol. 46, no. 2, pp. 194 –203, feb 1998. 9

- [22] J. Parsons and A. Sheikh, “The characterization of impulsive noise and considerations for a noise-measuring receiver,” *Radio and Electronic Engineer*, vol. 49, no. 9, pp. 467–476, september 1979. 9
- [23] G. Bedicks, C. Dantas, F. Sukys, F. Yamada, L. Raunheite, and C. Akamine, “Digital signal disturbed by impulsive noise,” *Broadcasting, IEEE Transactions on*, vol. 51, no. 3, pp. 322–328, sept. 2005. 9
- [24] A. Chandra, “Measurements of radio impulsive noise from various sources in an indoor environment at 900 mhz and 1800 mhz,” in *Personal, Indoor and Mobile Radio Communications, 2002. The 13th IEEE International Symposium on*, vol. 2, sept. 2002, pp. 639–643 vol.2. 9
- [25] A. Spaulding, “The natural and man-made noise environment in personal communications services bands,” *Institute for Telecommunication Sciences*, pp. 1–30, May 1997. 9
- [26] R. Owen, W. Vincent, and W. Blair, “Measurement of impulsive noise on electric distribution systems,” *Power Apparatus and Systems, IEEE Transactions on*, vol. PAS-99, no. 6, pp. 2433–2438, nov. 1980. 9
- [27] S. Nakamura, “A study of errors caused by impulsive noise and a simple estimation method for digital mobile communications,” *Vehicular Technology, IEEE Transactions on*, vol. 45, no. 2, pp. 310–317, may 1996. 10
- [28] E. N. Skomal and A. A. Smith, “Measuring the radio frequency environment,” vol. 26, no. 3, pp. 773–781, 1985. 10

- [29] T. Nakai and Z. Kawasaki, “Automotive noise from a motorway: Part i, measurement,” *Electromagnetic Compatibility, IEEE Transactions on*, vol. EMC-26, no. 4, pp. 169–174, nov. 1984. 10
- [30] T. Nakai, “Automotive noise from a motorway: Part ii, analysis,” *Electromagnetic Compatibility, IEEE Transactions on*, vol. EMC-26, no. 4, pp. 175–182, nov. 1984. 10
- [31] P. Bello, “Error probabilities due to atmospheric noise and flat fading in hf ionospheric communication systems,” *Communication Technology, IEEE Transactions on*, vol. 13, no. 3, pp. 266–279, september 1965. 10
- [32] E. Bolton, “Man-made noise study at 76 and 200 khz,” *Electromagnetic Compatibility, IEEE Transactions on*, vol. EMC-18, no. 3, pp. 93–96, aug. 1976. 10
- [33] A. D. SPAULDING and R. T. DISNEY, “Manmade radio noise part i: Estimates for business, residential and rural areas,” *U.S. DEPARTMENT OF COMMERCE*, pp. 1–148, june. 1974. 10
- [34] P. Bello and R. Esposito, “A new method for calculating probabilities of errors due to impulsive noise,” *Communication Technology, IEEE Transactions on*, vol. 17, no. 3, pp. 368–379, june 1969. 10
- [35] J. Cortes, L. Diez, F. Canete, and J. Lopez, “Analysis of the periodic impulsive noise asynchronous with the mains in indoor plc channels,” in *Power Line Communications and Its Applications, 2009. ISPLC 2009. IEEE International Symposium on*, 2009, pp. 26–30. 11

- [36] A. Papoulis and S. Pillai, “Probability, random variables, and stochastic processes,” *McGraw Hill*, Jan 2002. 11
- [37] A. Papoulis, *Probability, Random Variables, and Stochastic Processes*. McGraw-Hill Inc., 1991. 13
- [38] R. Ahlswede, N. Cai, S.-Y. Li, and R. Yeung, “Network information flow,” *Information Theory, IEEE Transactions on*, vol. 46, no. 4, pp. 1204–1216, jul 2000. 15, 17
- [39] S. Katti, S. Gollakota, and D. Katabi, “Embracing wireless interference: analog network coding,” *SIGCOMM Comput. Commun. Rev.*, vol. 37, pp. 397–408, August 2007. [Online]. Available: doi.acm.org/10.1145/1282427.1282425 16
- [40] Z. Li, X.-G. Xia, and B. Li, “Achieving full diversity and fast ml decoding via simple analog network coding for asynchronous two-way relay networks,” *Communications, IEEE Transactions on*, vol. 57, no. 12, pp. 3672–3681, 2009, December. 16
- [41] E. Peh, Y.-C. Liang, and Y. L. Guan, “Power control for physical-layer network coding in fading environments,” in *Personal, Indoor and Mobile Radio Communications, 2008. PIMRC 2008. IEEE 19th International Symposium on*, 2008, pp. 1–5. 19
- [42] J. Proakis, *Digital Communications*. McGrawHills, 2000. 22, 47, 70
- [43] A. Darmawan, S. Kim, and H. Morikawa, “Amplify-and-forward scheme in cooperative spatial multiplexing,” in *Mobile and Wireless Communications Summit, 2007. 16th IST*, 2007, pp. 1–5. 24
- [44] S. Hayakin, *Communication systems*, 1994. 30

- [45] T. Koike-Akino, P. Popovski, and V. Tarokh, “Optimized constellations for two-way wireless relaying with physical network coding,” *Selected Areas in Communications, IEEE Journal on*, vol. 27, no. 5, pp. 773–787, june 2009. 31
- [46] S. Alamouti, “A simple transmit diversity technique for wireless communications,” *Selected Areas in Communications, IEEE Journal on*, vol. 16, no. 8, pp. 1451–1458, oct 1998. 39
- [47] D. To, J. Choi, and I.-M. Kim, “Error probability analysis of bidirectional relay systems using alamouti scheme,” *Communications Letters, IEEE*, vol. 14, no. 8, pp. 758–760, 2010. 43
- [48] D. Gunduz, A. Goldsmith, and H. Poor, “Mimo two-way relay channel: Diversity-multiplexing tradeoff analysis,” in *Signals, Systems and Computers, 2008 42nd Asilomar Conference on*, 2008, pp. 1474–1478. 53
- [49] R. Pabst, B. H. Walke, D. Schultz, P. Herhold, H. Yanikomeroglu, S. Mukherjee, H. Viswanathan, M. Lott, W. Zirwas, M. Dohler, H. Aghvami, D. Falconer, and G. Fettweis, “Relay-based deployment concepts for wireless and mobile broadband radio,” *Communications Magazine, IEEE*, vol. 42, no. 9, pp. 80–89, Sept. 2004. 57
- [50] C. A. Balanis, *Antenna Theory: Analysis and Design, 3rd Edition*. Wiley, 2005. 59, 60
- [51] S. Ramo, *Fields and Waves in Communication Electronics*. Wiley, 1994. 60
- [52] H. Bolcskei, R. Nabar, V. Erceg, D. Gesbert, and A. Paulraj, “Performance of spatial multiplexing in the presence of polarization diversity,” in *Acoustics*,

- Speech, and Signal Processing, 2001. Proceedings. (ICASSP '01). 2001 IEEE International Conference on*, vol. 4, 2001, pp. 2437–2440 vol.4. 62
- [53] C. Oestges, V. Erceg, and A. Paulraj, “Propagation modeling of mimo multipolarized fixed wireless channels,” *Vehicular Technology, IEEE Transactions on*, vol. 53, no. 3, pp. 644–654, 2004. 62
- [54] J. D. Parsons, *The Mobile Radio Propagation Channel, 2nd Edition*, 2000. 63
- [55] T. S. Rappaport, *Wireless Communications: Principles and Practice (2nd Edition)*, 2001. 63
- [56] H. Asplund, J. E. Berg, F. Harrysson, J. Medbo, and M. Riback, “Propagation characteristics of polarized radio waves in cellular communications,” in *Vehicular Technology Conference, 2007. VTC-2007 Fall. 2007 IEEE 66th*, 2007, pp. 839–843. 66
- [57] M. K. S. abd Mohamed-Slim Alouini, *Digital Communication over Fading Channels (2nd Edition)*, 2000. 68, 69
- [58] S. Stein, “Unified analysis of certain coherent and noncoherent binary communications systems,” *Information Theory, IEEE Transactions on*, vol. 10, no. 1, pp. 43–51, 1964. 69
- [59] M. Fitz, “Further results in the unified analysis of digital communication systems,” *Communications, IEEE Transactions on*, vol. 40, no. 3, pp. 521–532, 1992. 69
- [60] L.-L. Yang and H.-H. Chen, “Error probability of digital communications using relay diversity over nakagami-m fading channels,” *Wireless Communications, IEEE Transactions on*, vol. 7, no. 5, pp. 1806–1811, 2008. 70

-
- [61] I. Gradshteyn and I. Ryzhik, *Table of Integrals, Series, and Products, Seventh Edition*, 2007. 71, 72, 73, 74
- [62] M. Hasna and M.-S. Alouini, “End-to-end performance of transmission systems with relays over rayleigh-fading channels,” *Wireless Communications, IEEE Transactions on*, vol. 2, no. 6, pp. 1126–1131, 2003. 73
- [63] N. Ferdinand and N. Rajatheva, “Performance analysis of imperfect channel estimation in mimo two hop fixed gain relay network with beamforming,” *Communications Letters, IEEE*, vol. 15, no. 2, pp. 208–210, 2011. 73
- [64] L. Jiang, L. Thiele, A. Brylka, S. Jaeckel, and V. Jungnickel, “Polarization characteristics of multiple-input multiple-output channels,” in *Personal, Indoor and Mobile Radio Communications, 2008. PIMRC 2008. IEEE 19th International Symposium on*, 2008, pp. 1–5. 79
- [65] B. Lindmark and M. Nilsson, “On the available diversity gain from different dual-polarized antennas,” *Selected Areas in Communications, IEEE Journal on*, vol. 19, no. 2, pp. 287–294, 2001. 81
- [66] A. M. d. Turkmani, A. Arowojolu, P. A. Jefford, and C. J. Kellett, “An experimental evaluation of the performance of two-branch space and polarization diversity schemes at 1800 mhz,” *Vehicular Technology, IEEE Transactions on*, vol. 44, no. 2, pp. 318–326, 1995. 81

Curriculum Vitae

Name: Siamack Ghadimi

Place of birth: Sepahan (Esfahan), Iran

Post-secondary Education and Degrees:

2010-2013 Ph.D.
Electrical Engineering
Western University
London, Ontario, Canada

1990-1995 B.Sc. and M.Sc.
Electrical Engineering
Lund University (LTH)
Lund, Sweden

Publications:

- [1] Siamack Ghadimi and Jamil Hussian, 'Effect of Impulsive Noise on Wireless Relay Channel" Wireless Sensor Network, 2012, 4, 167-172.